RadioGraphics

Imaging of Primary Chest Wall Tumors with Radiologic-Pathologic Correlation[1]

Se Jin Nam, MD • Sungjun Kim, MD • Beom Jin Lim, MD • Choon-Sik Yoon, MD • Tae Hoon Kim, MD • Jin-Suck Suh, MD • Doo Hoe Ha, MD Jong Won Kwon, MD • Young Cheol Yoon, MD • Hye Won Chung, MD Mi Sook Sung, MD • Yun Sun Choi, MD • Jang Gyu Cha, MD

ONLINE-ONLY CME

See www.rsna.org/education/rg_cme.html

LEARNING OBJECTIVES

After reading this article and taking the test, the reader will be able to:

- Describe common primary chest wall tumors in terms of location, origin, tissue components, and clinical features.
- Identify chest wall tumors on the basis of their MR imaging and CT appearances.
- Discuss imaging findings that facilitate the differential diagnoses of bone and soft-tissue tumors.

TEACHING POINTS

See last page

Neoplasms and tumorlike lesions that originate from chest wall tissues are uncommon compared with tumors in other parts of the body, and unfamiliarity with these disease entities can cause diagnostic difficulties for radiologists. Furthermore, the imaging features of many of these tumors are nonspecific, particularly those that are locally aggressive. However, a systematic approach based on patient age, clinical history, lesion location, and characteristic imaging findings often helps limit the differential diagnosis. Primary chest wall tumors can be classified as bone or soft-tissue tumors, with the latter being further classified into adipocytic tumors, vascular tumors, peripheral nerve sheath tumors, cutaneous lesions, fibroblastic-myofibroblastic tumors, and so-called fibrohistiocytic tumors, largely based on the 2002 World Health Organization classification. Within each category, it is possible to further limit the differential diagnosis with cross-sectional imaging. Information on specific features (eg, mineralization, fibrosis, hemosiderin deposits) and imaging patterns (eg, the "target sign" and "fascicular sign" seen in neurogenic tumors) can aid in making the diagnosis. Radiologists can achieve a sufficiently specific diagnosis of bone tumors and soft-tissue tumors if typical findings are present.

Abbreviations: ABC = aneurysmal bone cyst, DFSP = dermatofibrosarcoma protuberans, GCT = giant cell tumor, H-E = hematoxylin-eosin, PNST = peripheral nerve sheath tumor, UPS = undifferentiated pleomorphic sarcoma, WHO = World Health Organization

RadioGraphics 2011; 31:749–770 • **Published online** 10.1148/rg.313105509 • **Content Codes:** CH MK

[1]From the Departments of Radiology (S.J.N., S.K., C.S.Y., T.H.K.) and Pathology (B.J.L.), Gangnam Severance Hospital, Yonsei University, 146-92 Dogok-Dong, Gangnam-Gu, Seoul 135-720, Republic of Korea; Department of Radiology and Research Institute of Radiological Science, Severance Hospital, Yonsei University, Seoul, Republic of Korea (J.S.S.); Department of Radiology, CHA Bundang Medical Center, CHA University, Seongnam, Gyeonggi-do, Republic of Korea (D.H.H.); Department of Radiology and Center for Imaging Science, Samsung Medical Center, Sungkyunkwan University School of Medicine, Seoul, Republic of Korea (J.W.K., Y.C.Y.); Department of Radiology and Research Institute of Radiology, University of Ulsan College of Medicine, Asan Medical Center, Seoul, Republic of Korea (H.W.C.); Department of Radiology, Bucheon St Mary Hospital, The Catholic University of Korea, Bucheon, Gyeonggi-do, Republic of Korea (M.S.S.); Department of Radiology, Eulji Hospital, Eulji University School of Medicine, Seoul, Republic of Korea (Y.S.C.); and Department of Radiology, Bucheon Hospital, Soonchunhyang University, Bucheon, Gyeonggi-do, Republic of Korea (J.G.C.). Presented as an education exhibit at the 2009 RSNA Annual Meeting. Received February 2, 2010; revision requested March 24; final revision received July 30; accepted August 3. Supported by a faculty research grant from the Yonsei University College of Medicine for 2009 (No. 6-2009-0119). For this CME activity, the authors, editors, and reviewers have no relevant relationships to disclose. **Address correspondence to** S.K. (e-mail: *agn70@yuhs.ac*).

Introduction

Tumors that arise from the chest wall (including bone structures such as the sternum, clavicle, scapula, and ribs) or from adjacent soft tissues are less common than are tumors in other parts of the body (1,2). The resulting unfamiliarity can make it difficult for radiologists to limit the number of possible diagnoses. Furthermore, although some primary tumors of the chest wall demonstrate characteristic imaging features, many such tumors have nonspecific characteristics.

Lesions must be categorized to provide a meaningful, practical diagnostic approach, but any categorization of the diverse tumorous conditions that affect the chest wall is arbitrary. Nevertheless, we believe that classic categorizations on the basis of tumor origin and tissue components are helpful. Accordingly, we characterize primary chest wall tumors as either bone tumors or soft-tissue tumors. We subdivide bone tumors into malignant and benign lesions, and soft-tissue tumors (which are more varied) into six categories, four of which—adipocytic tumors, vascular tumors, fibroblastic-myofibroblastic tumors, and so-called fibrohistiocytic tumors—appear in the 2002 World Health Organization (WHO) classification system for soft-tissue tumors (3). Our fifth and sixth categories, peripheral nerve sheath tumors (PNSTs) and cutaneous lesions, are not included in the WHO classification system for soft-tissue tumors but were adopted because it is possible to limit the differential diagnosis of these lesions on the basis of *(a)* characteristic imaging findings or *(b)* tissue layer of origin. The WHO classification system actually categorizes soft-tissue tumors into nine different groups. The five groups in the WHO classification system that we did not use—smooth muscle tumors, pericytic tumors, skeletal muscle tumors, chondro-osseous tumors, and tumors of uncertain differentiation—often do not demonstrate specific imaging features or occur only very rarely on the chest wall, and they are not discussed in this article.

Instead, we discuss the radiologic, pathologic, and clinical features—which are important for limiting the differential diagnosis—of lesions that more commonly involve the chest wall or that have relatively characteristic imaging features at magnetic resonance (MR) imaging or computed tomography (CT).

Approach to Chest Wall Tumors

Irrespective of whether chest wall tumors arise from bone or soft tissue, many tumor entities largely exhibit nonspecific imaging features. However, substantial numbers of primary bone and soft-tissue tumors of the chest wall can be specifically diagnosed. The following criteria can aid in limiting the differential diagnosis of chest wall tumors: *(a)* overall prevalence and characteristic clinical features, *(b)* mineralization patterns (if any), *(c)* location at the chest wall, and *(d)* intrinsic MR imaging characteristics that correspond with histopathologic findings. As a diagnostic aid, we have summarized the key clinical, radiologic, and pathologic features of these lesions in Tables 1 and 2. A bulky mass invading adjacent structures but demonstrating neither specific signal intensity characteristics at MR imaging nor mineralization usually raises suspicion for a malignant bone or soft-tissue tumor, such as metastasis or sarcoma. However, when mineralization is present within a bulky mass, osteosarcoma and chondrosarcoma should be suspected. Benign bone tumors, which typically do not demonstrate extraosseous mass formation, may have imaging features that are specific enough to allow a pathologic diagnosis. These tumors include fibrous dysplasia (amorphous mineralization), osteochondroma (continuity of the medullary cavity between the lesion and affected bone), and enchondroma (benign osteolytic lesion with chondroid calcification). The following benign soft-tissue tumors have a distinct imaging appearance: lipoma (mature fat tissue on T1-weighted MR images), hemangioma (high signal intensity on T2-weighted images, a variable amount of fat tissue on T1-weighted images, and a phlebolith on CT scans), neurogenic tumor ("target sign" and "fascicular sign" on T2-weighted images), epidermal cyst (no high signal intensity on T2-weighted images), pilomatricoma (a calcified subdermal nodule with peritumoral edema on MR images), and elastofibroma (a fibrous mass located under the serratus anterior or latissimus dorsi muscle).

Bone Tumors

Metastatic bone tumors—including skeletal tumors of the chest wall—are the most commonly encountered type of skeletal tumor, particularly in older patients (4). On the other hand, primary bone tumors of the chest wall are uncommon, accounting for only 5%–8% of all skeletal masses (5). Furthermore, approximately 95% of these primary bone tumors are located in ribs, with most of the remainder in the sternum (6). In this article, we consider the ribs, sternum, scapula, and clavicle to be bones of the chest wall. It should be remembered that sternal tumors are usually malignant, whereas rib lesions have an equal likelihood of benignancy or malignancy (7).

Table 1
Key Clinical, Radiologic, and Pathologic Features of Primary Bone Tumors of the Chest Wall

Tumor	Frequency, Patient Age,* Mineralization	Signal Intensity† at T1-weighted MR Imaging	Signal Intensity† at T2-weighted MR Imaging	Notable MR Imaging Feature or Typical Location
		Malignant Tumors		
Myeloma	Common, ≥50 y, rare	Iso- to hypointense	Hyperintense	Nonspecific
Chondrosarcoma	Common, ≥50 y, chondroid (predilection for periphery)	Hypointense in area of mineralization against an iso- to hypointense background due to cartilage	Hypointense in area of mineralization against a bright background due to cartilage	Most frequently involves upper five ribs and the anterior chest wall
Osteosarcoma	Rare, ≤20 y, osteoid (predilection for center)	Hypointense in area of mineralization, sometimes hyperintense due to mineralization or hemorrhage	Variably intense, hypointense in area of mineralization	Costochondral junction
Parosteal osteosarcoma	Rare, 20–30 y, dense calcification	Hypointense due to dense mineralization	Hypointense due to dense mineralization	Mainly extraosseous with minimal (if any) medullary involvement
Ewing sarcoma	Rare, 0–20 y, rare	Hyperintense in area of hemorrhage	Heterogeneously hyperintense	Intense enhancement
		Benign Tumors		
Fibrous dysplasia	Common, 20–30 y, ground glass–like, amorphous	Iso- to hypointense	Variably intense due to various pathologic components	Expansile, no extraosseous mass; posterior arc of rib
Enchondroma	Uncommon, 20–40 y, chondroid	Hypointense in area of mineralization, sometimes hyperintense due to mineralization or hemorrhage	Variably intense, hypointense in area of mineralization	Septal and peripheral enhancement; costochondral junction
Osteochondroma	Uncommon, 10–40 y, occasionally seen at cartilage cap	Isointense‡	Hyperintense cartilage cap	Continuity with medullary cavity of affected bone; costochondral junction
Chondroblastoma	Rare, 10–20 y (patients with rib lesions are older), chondroid (25%–50%)	Hypointense in area of mineralization against an iso- to hypointense background due to cartilage	Hypointense in area of mineralization against a bright background due to cartilage	ABC change, edema of adjacent bone and soft tissue
ABC	Uncommon, 20–40 y, almost never seen	Heterogeneously intense due to hemorrhage	Heterogeneously intense due to hemorrhage	Fluid level
GCT	Uncommon, 20–40 y, almost never seen	Iso- to hypointense	Heterogeneously intense, hypointense due to hemosiderin or fibrosis	Fluid-fluid level in ABC change

Note.—ABC = aneurysmal bone cyst, GCT = giant cell tumor.
*Age at which tumor is most frequently recognized. †Relative to muscle. ‡Relative to medullary cavity of affected bone, except for the cartilage cap, which is isointense relative to muscle.

Table 2
Key Clinical, Radiologic, and Pathologic Features of Primary Soft-Tissue Tumors of the Chest Wall

Tumor	Frequency, Patient Age,* Mineralization	Signal Intensity† at T1-weighted MR Imaging	Signal Intensity† at T2-weighted MR Imaging	Notable MR Imaging Feature or Typical Location
		Adipocytic Tumors		
Lipoma	Common, 40–50 y, uncommon	Hyperintense	Hyperintense	Thin septa
Liposarcoma	Common, 40–50 y, uncommon	Hyperintense (variable amount of fat tissue depending on histologic type)	Hyperintense (varied amount of fat tissue according to histologic type)	Thick septa, <75% fat
		Vascular Tumors		
Hemangioma	Uncommon, 0–30 y, phleboliths (20%–67%)	Heterogeneous with hyperintense spot (fat tissue)	Heterogeneous with hyperintense spot (fat tissue), bright vascular space	Variable enhancement
Lymphangioma	Uncommon, 1–2 y, rare	Iso- to hypointense	Bright	Not applicable
Angiosarcoma	Rare, ≥60 y, no calcification	Heterogeneous	Heterogeneous	Associated with lymphedema
		PNSTs		
Schwannoma	Common, 20–50 y, uncommon	Iso- to hypointense	Heterogeneous signal intensity with a ring-like pattern (fascicular sign)‡	Degeneration (more common than in neurofibroma)
Neurofibroma	Common, 20–30 y, less common than in schwannoma	Iso- to hypointense	Central hypointensity and peripheral hyperintensity (target sign)‡	Degeneration (more common in schwannoma)
Malignant PNST	Uncommon, 20–50 y, no calcification	Iso- to hyperintense	Heterogeneously hyperintense	Frequent absence of target sign or fascicular sign

(Table 2 continues)

Teaching Point

Chondrosarcoma is the most common primary malignant bone tumor of the chest wall and accounts for 33% of all primary rib tumors, with myeloma being the second most common. Ewing sarcoma is the most common primary bone tumor in children (1,8–10). Fibrous dysplasia is the most common benign tumorous condition of the osseous chest wall, accounting for approximately 30% of these tumors (11).

Malignant Bone Tumors

Traditionally, bone tumors that demonstrate extensive cortical destruction and extraosseous soft-tissue mass formation have been categorized as malignant. Bone destruction is better depicted with CT, whereas extraosseous mass formation is better visualized at MR imaging. When a malignant bone tumor does not have any specific imaging features and demonstrates only the typical features of a malignant lesion, limiting the differential diagnosis is difficult. The imaging features that aid in limiting the differential diagnosis of primary malignant tumors are described in the remainder of this section, with a focus on mineralization and signal intensity characteristics at MR imaging.

Mineralization in the matrix of a presumably malignant tumor is useful diagnostic information, making CT an important diagnostic tool. When mineralization shows typical chondroid features, such as an arc-and-ring appearance, flocculence, or a stippled shape, chondrosarcoma should be considered. The pattern of mineralization in chondrosarcoma has been described as nodular and peripheral (Fig 1) (12,13). On the other

Table 2 *(continued)*
Key Clinical, Radiologic, and Pathologic Features of Primary Soft-Tissue Tumors of the Chest Wall

Tumor	Frequency, Patient Age,* Mineralization	Signal Intensity† at T1-weighted MR Imaging	Signal Intensity† at T2-weighted MR Imaging	Notable MR Imaging Feature or Typical Location
		Cutaneous Lesions		
Epidermal inclusion cyst	Common, any age, may be present	Variable, occasionally hyperintense due to calcification	Variable (not bright, even though a cyst)	Peripheral enhancement at the wall, subdermal location
Pilomatricoma	Common, 0–20 y (40%); peak, 10–15 y, typically central (80%)	Homogeneously isointense	Heterogeneous and variable	Peripheral enhancement at the capsule, subdermal location
DFSP	Uncommon, 20–40 y, no calcification	Hypointense	Hyperintense§	Confined to subdermal location (if small)
		Fibroblastic-Myofibroblastic Tumors		
Elastofibroma	Common, 50–60 y, no calcification	Isointense with interspersed fat streak	Isointense with interspersed fat streak	Bilateral (10%–66%), near the lower tip of the scapula
Fibromatosis	Common, 10–40 y; peak, 25–35 y, no calcification	Hypointense due to fibrous streak suggesting fibrosis and a myxoid component	Heterogeneous and hypointense due to fibrous streak suggesting fibrosis and a myxoid component	Infiltrating margin, heterogeneous enhancement
		So-called Fibrohistiocytic Tumors		
UPS	Uncommon, ≥40 y, unusual	Isointense	Iso- to hyperintense§	Heterogeneous enhancement

Note.—DFSP = dermatofibrosarcoma protuberans, PNST = peripheral nerve sheath tumor, UPS = undifferentiated pleomorphic sarcoma. *Age at which tumor is most frequently recognized. †Relative to muscle. ‡Substantial overlap between the target sign and the fascicular sign. §Relative to fat.

Figure 1. Chondrosarcoma in a 36-year-old woman. **(a)** Contrast material–enhanced CT scan obtained at the level of the diaphragm shows a rib mass with chondroid calcifications and extensive extraosseous mass formation. **(b)** Photograph of the cut surface of the excised specimen shows a mass (maximum diameter, ~10 cm) consisting of glistening, whitish, lobular calcified cartilage (arrows), which corresponds to the calcifications seen at CT. The mass is seen invading adjacent tissue (arrowheads).

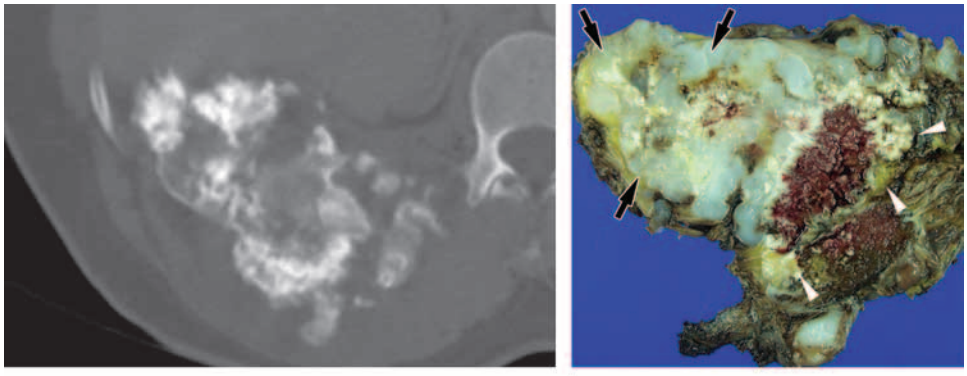

a. b.

Figure 2. Osteosarcoma in a 39-year-old man. **(a)** Noncontrast CT scan obtained at the level of the liver shows a rib mass (arrow) with central mineralization (arrowhead) near the costovertebral junction. **(b)** Axial T2-weighted MR image (repetition time msec/echo time msec = 3500/98) obtained at the same level more clearly depicts the extraosseous mass (arrowhead). **(c)** Photograph of the cut surface of the excised specimen shows an ill-defined mass with whitish internal foci at the center (arrowheads), findings that suggest osteoid mineralization.

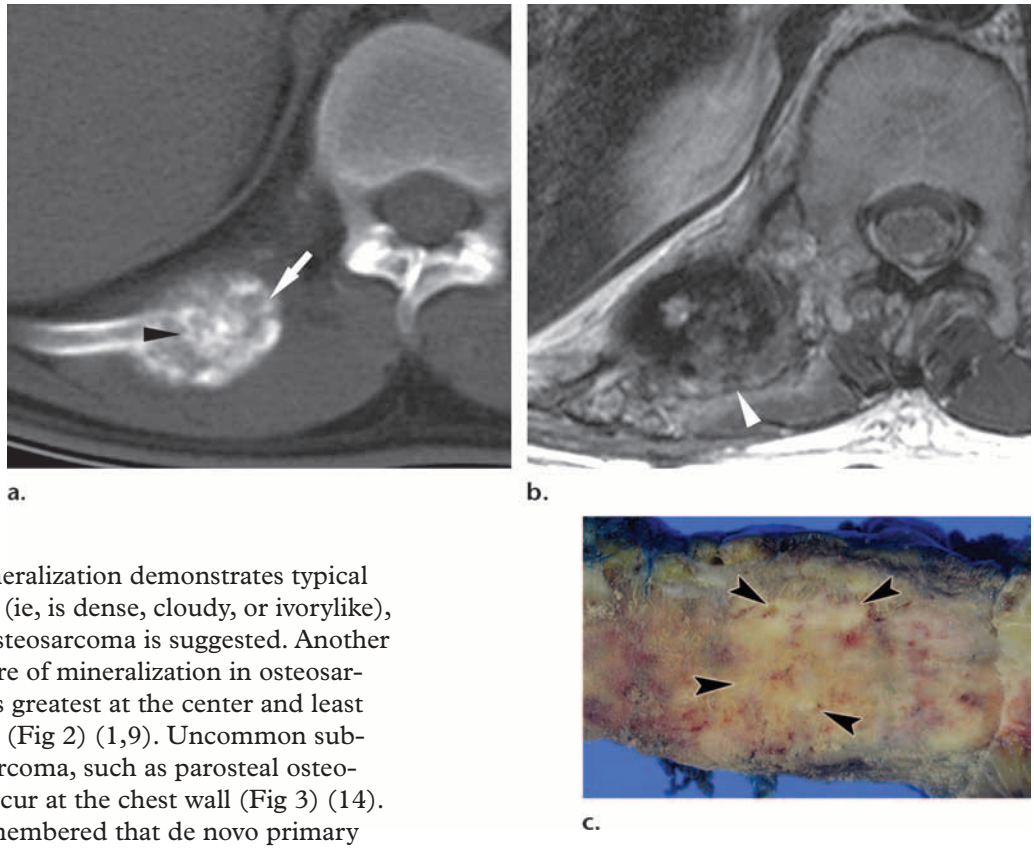

hand, when mineralization demonstrates typical osteoid features (ie, is dense, cloudy, or ivorylike), a diagnosis of osteosarcoma is suggested. Another important feature of mineralization in osteosarcoma is that it is greatest at the center and least at the periphery (Fig 2) (1,9). Uncommon subtypes of osteosarcoma, such as parosteal osteosarcoma, can occur at the chest wall (Fig 3) (14). It should be remembered that de novo primary osteosarcoma of the chest wall is rare, whereas chondrosarcoma is the most common primary malignant bone tumor of the chest wall. In a series of 1274 cases, osteosarcoma was reported to primarily involve the rib in only 1.3% (15). In the absence of mineralization, more common malignant bone tumors such as metastatic bone tumor, a hematologic malignancy, and myeloma should also be considered. Clinical history (patient age and underlying diseases) and imaging findings (signal intensity characteristics at MR imaging) aid in limiting the differential diagnosis. MR imaging sometimes allows further analysis of tissue contents. Chondrosarcomas may have high signal intensity on T2-weighted images, reflecting a hyaline cartilage matrix of uniform composition with high water content. Contrast enhancement with a peripheral and septal pattern is often present (16). Calcifications in tumors typically appear as signal voids with all MR pulse sequences, irrespective of disease. In osteosarcoma, mineralized portions of tumors have low signal intensity on T1- and T2-weighted images, whereas nonmineralized areas and soft-tissue tumors have high signal intensity on T2-weighted images (17).

Benign Bone Tumors

The three most frequently encountered benign chest wall lesions are fibrous dysplasia, osteochondroma, and enchondroma (18), whereas chondroblastoma, aneurysmal bone cyst (ABC), and giant cell tumor (GCT) are rare.

Fibrous Dysplasia.—Fibrous dysplasia is a developmental anomaly in which osteoblasts fail to undergo normal morphologic differentiation and maturation, leading to the replacement of normal marrow and cancellous bone by immature bone and fibrous stroma. Approximately 6%–20% of cases of monostotic fibrous dysplasia develop in the ribs, with 55% of cases of polyostotic fibrous

Figure 3. Parosteal osteosarcoma in a 41-year-old man. **(a)** Contrast-enhanced CT scan obtained at the midscapula level shows a mass (maximum diameter, ~7 cm) surrounding the scapula from both ventral and dorsal aspects. The mass is densely mineralized, and its mineralized portion (arrow) crosses the medullary cavity of the scapula, a finding that suggests medullary involvement. **(b)** Axial T2-weighted MR image (3200/98) obtained at the same level shows the mass (arrows) as a hypointense region, reflecting dense calcification. **(c)** Photograph of the cut surface of the excised specimen shows a compactly mineralized extraosseous tumor (arrowheads) with partial involvement of the medullary cavity.

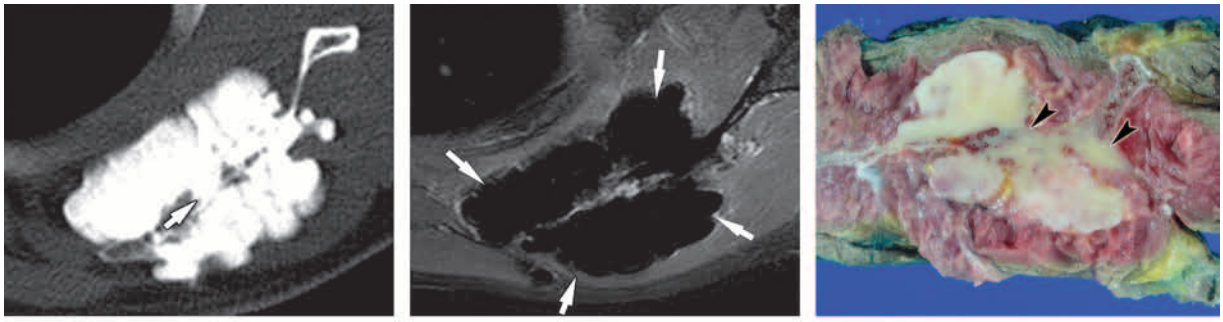

Figure 4. Fibrous dysplasia of a rib in a 17-year-old boy. **(a)** Noncontrast CT scan obtained at the level of the second rib shows a mass with expansile remodeling of a protracted length of bone. Trabeculation is seen at the periphery (arrowheads), but mineralization was not observed. **(b)** On a coronal T2-weighted MR image (4500/120), the tumor (arrowheads) demonstrates heterogeneous signal intensity. **(c)** Photomicrograph (original magnification, ×100; hematoxylin-eosin [H-E] stain) shows tissue with fibrous proliferation and osteoid formation, but without osteoblastic rimming (arrowheads).

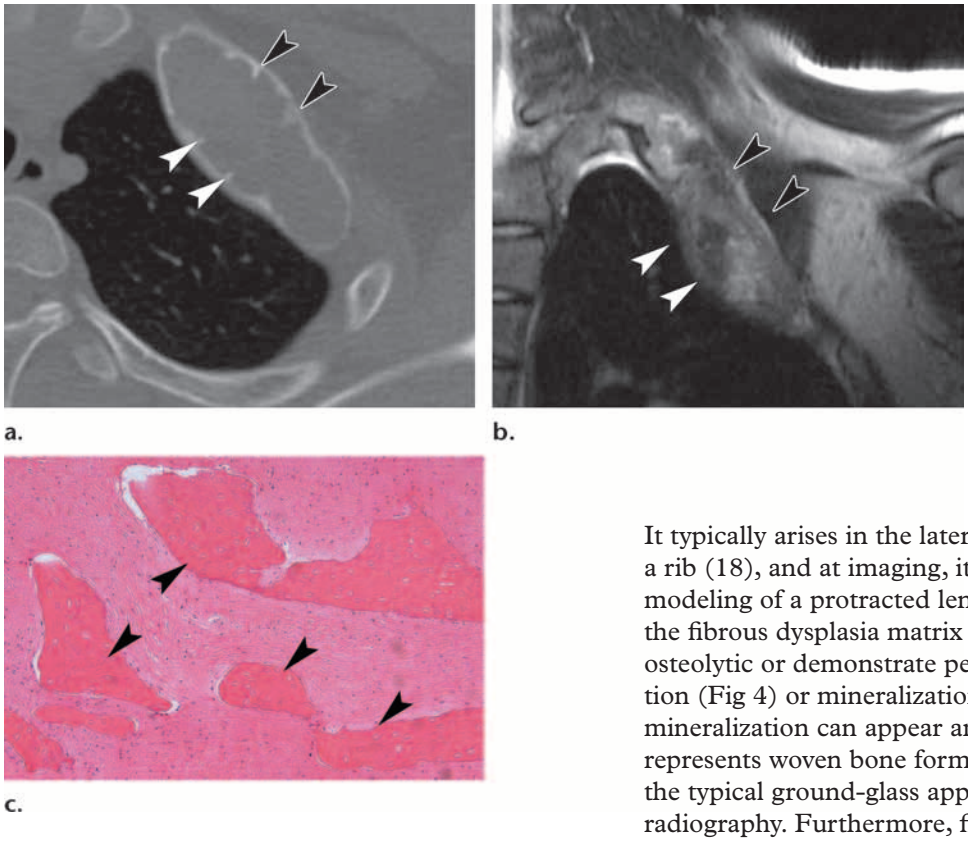

dysplasia demonstrating rib involvement (19). Fibrous dysplasia is the most common cause of an osteolytic lesion by a benign tumor or tumor-like lesion arising from the bone of the chest wall. It typically arises in the lateral or posterior arc of a rib (18), and at imaging, it shows expansile remodeling of a protracted length of bone. At CT, the fibrous dysplasia matrix may appear purely osteolytic or demonstrate peripheral trabeculation (Fig 4) or mineralization. Fibrous dysplasia mineralization can appear amorphous, which represents woven bone formation and creates the typical ground-glass appearance described at radiography. Furthermore, fibrous dysplasia can contain cartilage nodules, which may demonstrate typical cartilaginous mineralization (12). At MR imaging, various tissue components affect the

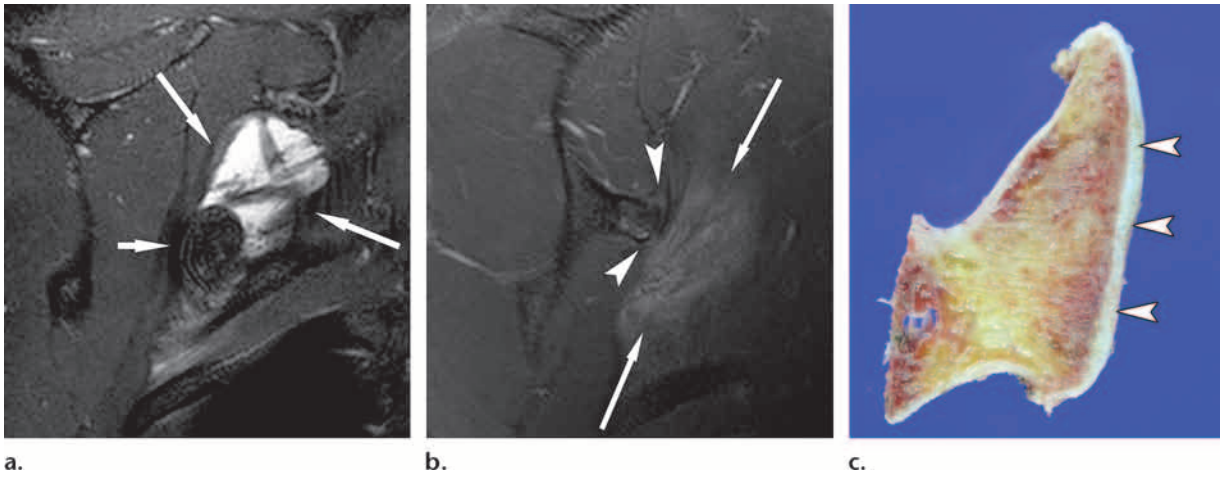

Figure 5. Osteochondroma of the scapula that resulted in scapulothoracic bursitis in an 18-year-old man. **(a)** Coronal fat-suppressed T2-weighted MR image (5000/120) of the right posterolateral side of the chest wall reveals osteocartilaginous exostosis (short arrow). Note the extensive scapulothoracic bursitis (long arrows) adjacent to the lesion, which was speculated to have resulted from irritation by the osteochondroma. **(b)** Coronal fat-suppressed T2-weighted MR image (5000/120) shows the lesion with a thin, hyperintense cartilage cap (arrowheads), along with scapulothoracic bursitis (arrows). **(c)** Photograph of the cut surface of the excised specimen shows the cartilage cap (arrowheads).

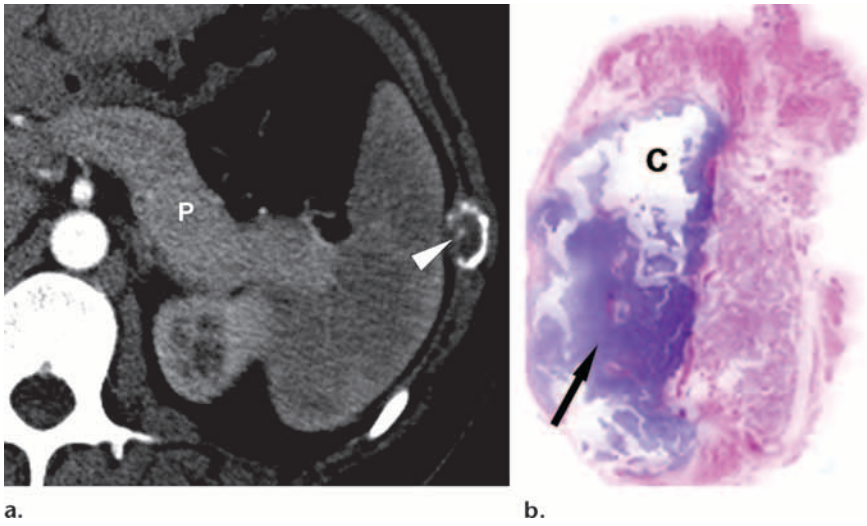

Figure 6. Enchondroma of a rib in a 25-year-old woman. **(a)** Contrast-enhanced CT scan shows a rib mass with cortical expansion at the costochondral junction. Note the punctate calcification (arrowhead), suggesting a chondroid matrix. *P* = pancreas. **(b)** Photograph of the cut surface of the excised specimen prepared for microscopic examination (H-E stain) shows a cartilage matrix (arrow). Cystic space *(C)* that remained after decalcification corresponds to the calcification seen at CT.

signal intensity characteristics of fibrous dysplasia. Generally, fibrous dysplasia has signal intensities ranging from low to high on T2-weighted images (Fig 4b), although in the majority of cases it has high signal intensity (20).

Osteochondroma.—Osteochondroma is a hamartomatous, cartilage-capped osseous growth that projects from the surface of the affected bone. Although one large series reported that solitary osteochondromas account for about 35%–41% of all benign bone tumors throughout the body (21), solitary osteochondromas involving a chest wall bone (rib, sternum, scapula, or clavicle) are relatively uncommon. In fact, only 8% of all rib tumors are osteochondromas (22), and in the ribs, osteochondromas show a predilection for the costochondral junction (23). When a solitary osteochondroma arises at the ventral side of the scapula, it sometimes causes pain related to bursa formation (Fig 5) (24). CT and MR imaging can both reveal continuity of the marrow cavity between the lesion and affected bone, the hallmark of osteochondroma. However, MR imaging is the most accurate technique for demonstrating a cartilage cap and for evaluating changes in involved adjacent structures. Cartilage caps have high signal intensity on T2-weighted images, as do the

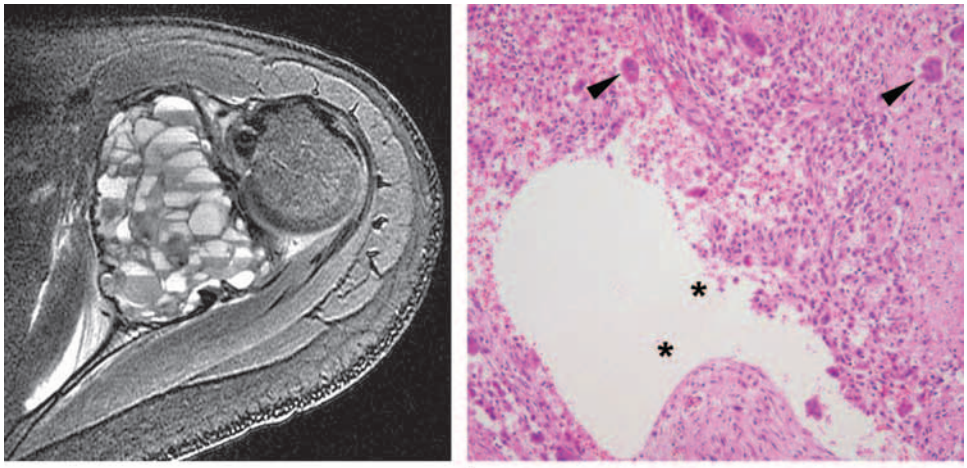

Figure 7. Primary ABC of the scapula in an 18-year-old woman. **(a)** Axial fat-suppressed T2-weighted MR image (4000/99) of the scapula shows a mass (maximum diameter, ~6.5 cm) affecting the left chest wall and consisting of multiple cysts with fluid levels. **(b)** Photomicrograph (original magnification, ×100; H-E stain) demonstrates osteoclast-like giant cells (arrowheads) with vacant spaces (*), which were believed to have been blood filled.

cartilaginous tissues of other tumors (23), and cartilage cap thickness is an important indicator of osteochondroma-to-sarcoma transformation. If the thickness of a cartilage cap exceeds 2 cm in adults or 3 cm in children, malignant transformation should be suspected (25).

Enchondroma.—Incarbone and Pastorino (18) reported enchondroma to be the second most common benign rib tumor after fibrous dysplasia. Enchondroma usually arises from cartilaginous tissue at the costochondral junction (18). CT reveals a slow-growing, lobulated, well-demarcated osteolytic lesion with or without bulging of cortical bone (Fig 6). Not all enchondromas demonstrate calcification at CT, and when calcification is not seen in the matrix, MR imaging is helpful. The high water content of hyaline cartilage produces high signal intensity on T2-weighted images, and the additional presence of a lobulated contour strongly suggests the possibility of enchondroma. However, enchondroma is generally considered to occur only rarely on the chest wall (7,26); chondrosarcoma is much more common. Hence, a destructive osseous lesion of the chest wall is initially suspected by the radiologist to be chondrosarcoma when mineralization is present (27).

Teaching Point

Chondroblastoma.—Chondroblastoma, which is usually found in the epiphyseal regions of long bones, can occur at the chest wall and involve the ribs or scapulae. Furthermore, whereas chondroblastoma of the long bones is most commonly encountered in the 2nd decade of life, chondroblastoma of the rib is normally encountered substantially later (28). Chondroblastoma typically arises at an ossification center, and therefore occurs at the costovertebral or costochondral junction (28). The imaging features of chondroblastoma can be aggressive and show ABC change, and it is sometimes difficult to exclude a malignant bone tumor. In addition, edema of adjacent bone marrow and soft tissue can be prominent.

Aneurysmal Bone Cyst.—ABCs can occur due to a secondary change of another bone tumor, but they can also occur as primary tumors. Most primary ABCs occur in patients under 30 years of age. At gross examination, masses are seen to contain a network of blood-filled cysts that histologic analysis shows to be lined with fibroblasts and multinucleated giant cells. Typically, MR imaging reflects the morphologic features of the tumor at gross examination and shows a lobulated or septated mass with a thin, well-defined rim of low signal intensity (29). Fluid levels are commonly seen within ABCs, indicating hemorrhage (Fig 7), but also occur in other tumors showing secondary ABC change; consequently, the presence of a fluid level is not pathognomonic (30).

Giant Cell Tumor.—GCTs are benign lesions composed of vascular sinuses lined or filled with abundant spindle and giant cells, and they tend

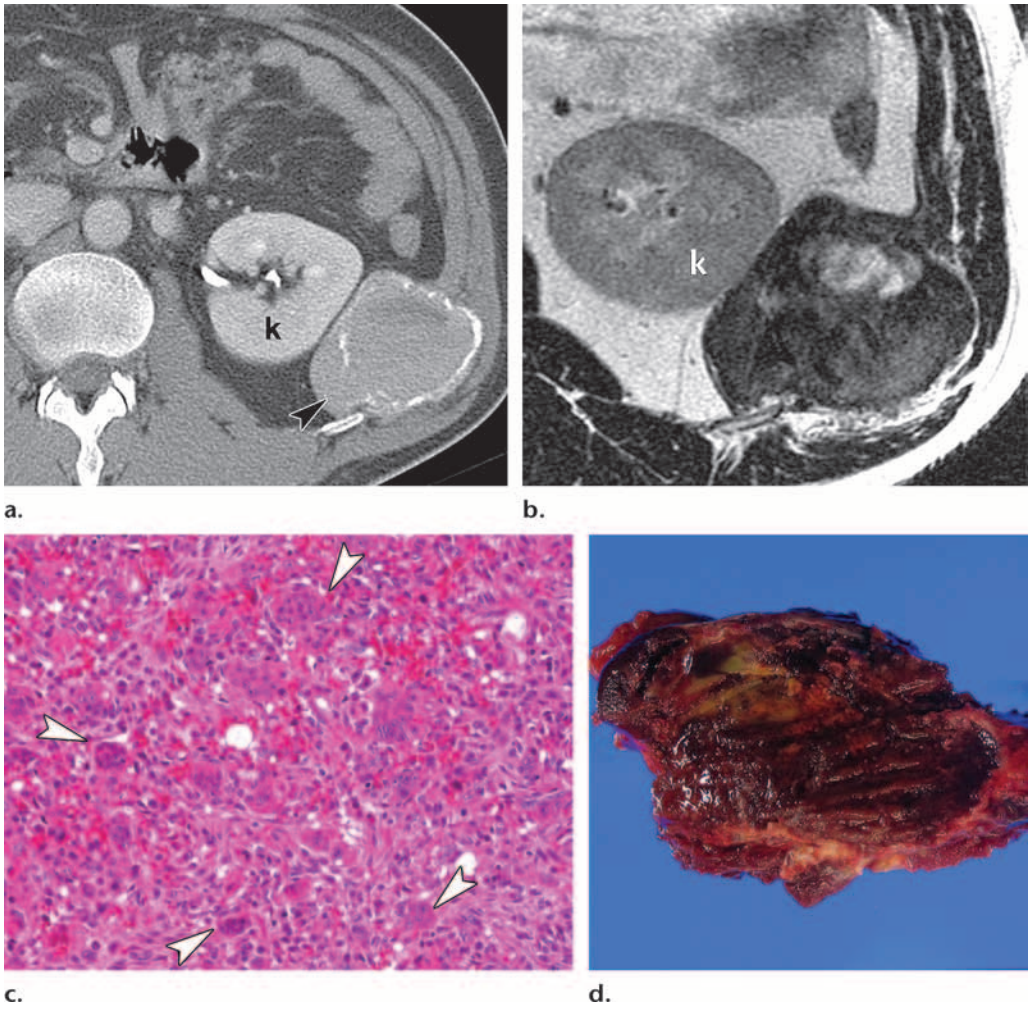

Figure 8. GCT of a rib in a 41-year-old man. **(a)** Contrast-enhanced CT scan obtained at the level of the kidney *(k)* shows a mass with an extraosseous portion (arrowhead) and accompanied by cortical destruction. Mineralization of the tumor was not observed. **(b)** On the corresponding axial T2-weighted MR image (3500/89), the tumor is heterogeneously dark, suggesting a fibrous component with or without chronic hemorrhage. *k* = kidney. **(c)** Photomicrograph (original magnification, ×200; H-E stain) reveals multinucleated giant cells (arrowheads). **(d)** Photograph of the cut surface of the excised specimen demonstrates friable fibrous tissue with hemorrhage.

to occur during the 3rd or 4th decade of life. GCTs of the chest wall often arise in the subchondral regions of flat and tubular bones, such as the sternum, clavicle, and ribs (23). They typically have low to intermediate signal intensity on T1- and T2-weighted MR images. However, one investigator stressed that they can have low signal intensity on these images, a finding that may reflect dense collagen and hemosiderin deposits within the tumor (Fig 8) (31,32). ABC changes are also common in GCTs.

Langerhans Cell Histiocytosis.—Generally, Langerhans cell histiocytosis involves the osseous chest wall and is seen in patients under 20 years of age. Solitary involvement of a rib is known to account for approximately 9.2%–15% of eosinophilic granulomas, which represent the mildest subtype of Langerhans cell histiocytosis. CT and MR imaging findings are nonspecific, but perilesional edema can be profound, especially in the early phase (33).

Soft-Tissue Tumors

Teaching Point

In adults, the most common benign soft-tissue neoplasm is lipoma, and the most common malignant neoplasm is undifferentiated pleomorphic sarcoma (UPS), a term that is used interchangeably with *malignant fibrous histiocytoma*. In children, rhabdomyosarcoma and primitive neuroectodermal tumor (Askin tumor) are the most common malignant soft-tissue tumors (26). Many soft-tissue neoplasms share similar characteristics

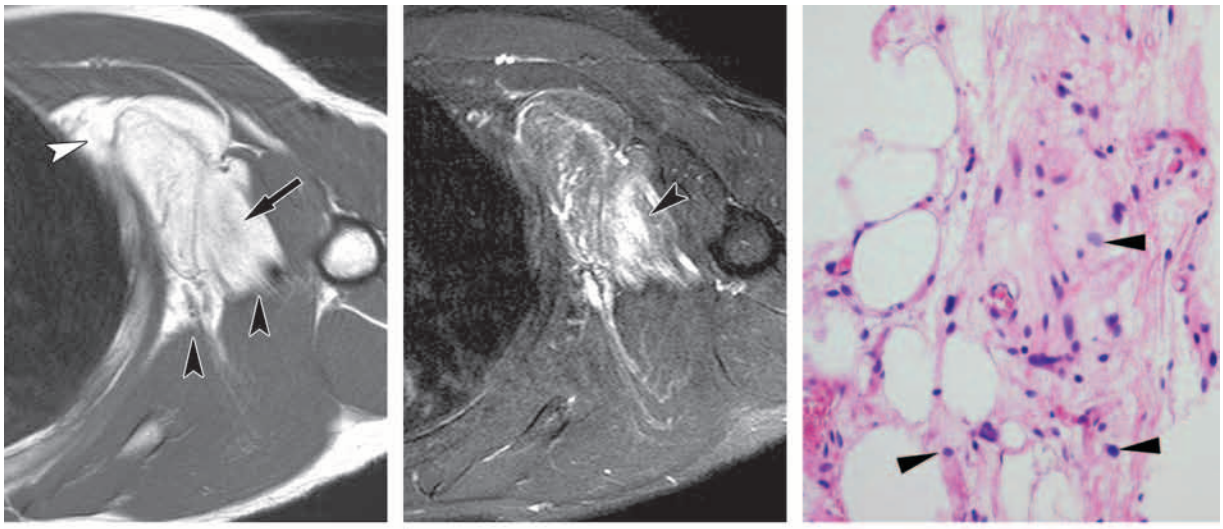

a. b. c.

Figure 9. Well-differentiated liposarcoma in a 51-year-old man. **(a)** Axial T1-weighted MR image (550/9) of the left chest wall shows a mass (maximum diameter, ~7.5 cm) superficial to the rib cage. The mass is well defined but shows marginal invasion of adjacent muscle and of the rib cage (arrowheads). Most of the tumor has high signal intensity. However, a nonfat component (arrow) is also seen, suggesting the presence of a malignant component. **(b)** Axial gadolinium-enhanced fat-suppressed T1-weighted MR image (550/9) shows diffuse streaky and nodular enhancement of the nonfat region of the tumor (arrowhead). **(c)** Photomicrograph (original magnification, ×200; H-E stain) reveals fat vacuoles that vary greatly in size. Note the adipocytic nuclear atypia (arrowheads) within the collagenous stroma and the relatively high density of vessels, findings that are believed to have caused the prominent enhancement seen on gadolinium-enhanced T1-weighted MR images (cf **b**).

at cross-sectional imaging, and the differentiation of sarcoma types frequently requires biopsy (7,26).

Adipocytic Tumors

Fatty tumors of the chest wall are relatively common, and although conventional lipoma is by far the most frequently encountered fatty soft-tissue tumor, there are a number of variants. In this article, however, we focus only on conventional lipoma and well-differentiated liposarcoma.

Lipoma.—Lipoma, the most common soft-tissue tumor, is most frequently observed in patients over 50 years of age. All lipomas are composed of adipose tissue, but various types of nonadipose tissue, such as connective tissue septa and calcification, are present in one-third of these tumors (34,35). On gadolinium-enhanced MR images, lipomas typically do not enhance. However, septa less than 2 mm in thickness are often visible and may enhance mildly (34,35). Furthermore, many lipomas of the chest wall are deep seated and involve deep intermuscular or muscular layers (34,35).

Liposarcoma.—Liposarcoma is the second most common subtype of chest wall soft-tissue malignancy after UPS (36). The WHO identifies five basic pathologic subtypes—well-differentiated, dedifferentiated, myxoid, pleomorphic, and mixed—and imaging findings of liposarcomas depend on the subtype (7). Well-differentiated liposarcoma is the most common subtype, accounting for approximately 50% of lesions (37). The WHO classification system treats atypical lipomatous tumor and well-differentiated liposarcoma as identical, since they share the same morphologic features, karyotype, and biologic behavior.

Typically, well-differentiated liposarcoma appears as a predominantly fatty lesion, with 50%–75% of tumor volume demonstrating fat signal intensity, and the MR imaging features of well-differentiated liposarcoma are frequently characteristic. Well-differentiated liposarcoma has been reported to have characteristic MR imaging features in 91%–96% of cases but to appear similar to lipoma in 4%–9% of cases (37). MR imaging features that suggest well-differentiated liposarcoma rather than lipoma include the presence of *(a)* prominent internal septa greater than 2 mm in thickness, and *(b)* nodular nonadipose areas (35). The gadolinium enhancement of nonadipose regions is variable (Fig 9) and has been described as ranging from mild to marked (35); however, one research group reported that the thick, irregular septa of liposarcomas enhance significantly in most cases, whereas thin septa enhance only faintly (38). Other histologic types

Teaching Point

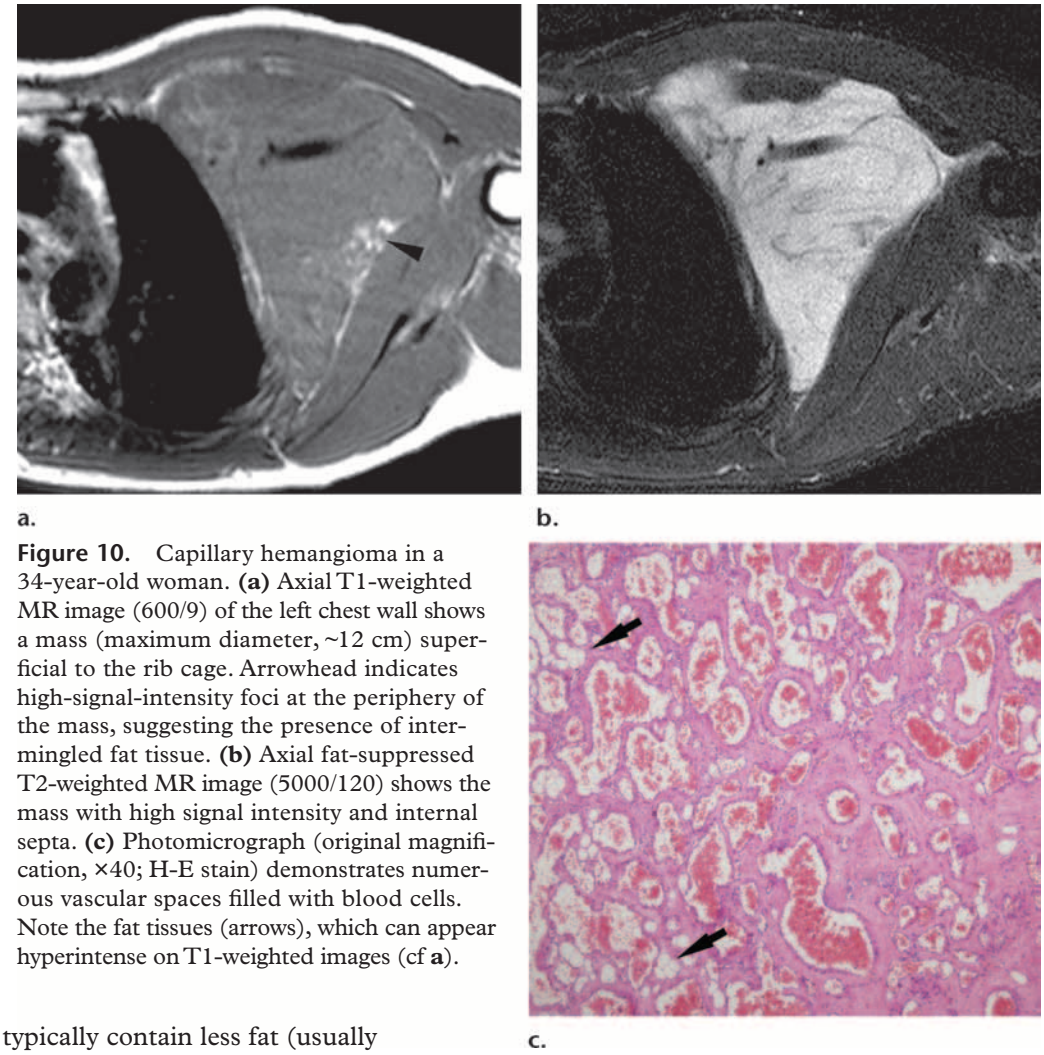

Figure 10. Capillary hemangioma in a 34-year-old woman. **(a)** Axial T1-weighted MR image (600/9) of the left chest wall shows a mass (maximum diameter, ~12 cm) superficial to the rib cage. Arrowhead indicates high-signal-intensity foci at the periphery of the mass, suggesting the presence of intermingled fat tissue. **(b)** Axial fat-suppressed T2-weighted MR image (5000/120) shows the mass with high signal intensity and internal septa. **(c)** Photomicrograph (original magnification, ×40; H-E stain) demonstrates numerous vascular spaces filled with blood cells. Note the fat tissues (arrows), which can appear hyperintense on T1-weighted images (cf **a**).

of liposarcoma typically contain less fat (usually less than 25% of tumor volume at cross-sectional imaging) (7), and pleomorphic liposarcomas have been reported to demonstrate no fat on MR images in 62%–75% of cases (7,39).

Vascular Tumors

Vascular tumors include benign tumors (eg, hemangioma, lymphangioma), tumors showing intermediate biologic behavior (eg, hemangioendothelioma), and malignant tumors (eg, angiosarcoma).

Hemangioma.—Hemangiomas are occasionally found in the soft tissue of the chest wall. Here, we use the term *hemangioma* in its broadest sense. Furthermore, we agree with other authors that these lesions represent benign nonreactive lesions with high numbers of normal- or abnormal-appearing vessels. At pathologic analysis, hemangiomas can be subclassified according to the predominant type of vascular channel (capillary, cavernous, arteriovenous, or venous) present within the lesion (40). However, subclassification is frequently difficult due to admixtures of histologic components. Hemangiomas also commonly manifest with nonvascular elements, which include fat, smooth muscle, thrombus, fibrous tissue, and hemosiderin. Phleboliths (dystrophic calcifications of thrombi) are most frequently observed in cavernous hemangiomas but can also be present in other vascular lesions (41). One CT study found that 30% of cavernous hemangiomas contain a phlebolith (42). At T1- and T2-weighted imaging, hemangiomas typically demonstrate regions of high signal intensity representing vascular tissue intermixed with variable (and sometimes substantial) amounts of fat (Fig 10) (7).

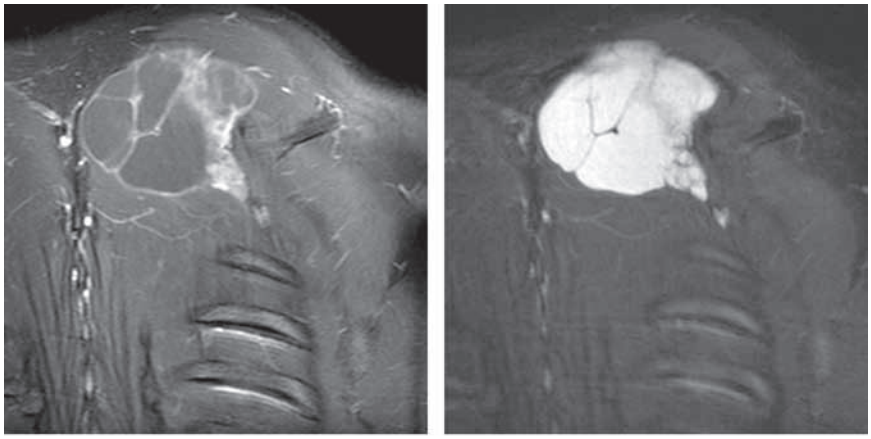

a. b.

Figure 11. Lymphangioma in a 19-year-old man. **(a)** Coronal gadolinium-enhanced fat-suppressed T1-weighted MR image (600/9) of the left posterior chest wall shows a thin peripheral rim and septal enhancement suggestive of multilocular cystic spaces. **(b)** Coronal fat-suppressed T2-weighted MR image (3500/80) obtained at the same level reveals a hyperintense lesion (maximum diameter, ~6 cm) with internal septa.

Lymphangioma.—Lymphangioma is a congenital lesion that consists of dilated lymphatic vessels and is commonly encountered in the neck and axilla, although it is most commonly found at the cervicothoracic junction in children and in the mediastinum in adults (7). Lesions are usually present at birth (50%–65% of cases) and nearly always by 2 years of age (90%) (40). Lymphangioma typically has low signal intensity similar to or less than that of muscle on T1-weighted MR images but high signal intensity greater than that of fat on T2-weighted images. There is thin peripheral and septal enhancement following gadolinium administration (Fig 11) (40).

Intermediate and Malignant Vascular Tumors.—Angiosarcoma is the most aggressive type of soft-tissue tumor arising from vascular tissue, and it usually affects adults. Chronic lymphedema is well known to predispose to angiosarcoma, although only approximately 10% of lesions demonstrate this association. The vast majority of angiosarcomas associated with lymphedema are found in postmastectomy patients (40). The imaging features of malignant vascular tumors (angiosarcomas and Kaposi sarcomas) and those of vascular tumors of intermediate aggressiveness (hemangioendotheliomas and hemangiopericytomas) are dependent on lesion location (ie, superficial or deep). Most superficial aggressive vascular tumors are Kaposi sarcomas or angiosarcomas, and cross-sectional imaging reveals skin thickening and subcutaneous edema with an associated focal soft-tissue mass. On the other hand, deep-seated malignant vascular tumors or vascular tumors of intermediate aggressiveness are usually hemangioendotheliomas, hemangiopericytomas, or angiosarcomas, any of which may have the nonspecific imaging appearance of a solid mass (40).

Peripheral Nerve Sheath Tumors

Neurogenic tumors of the chest wall arise from spinal nerve roots, intercostal nerves, and (sometimes) distal brachial plexus branches. The benign group includes schwannomas and neurofibromas; malignant PNSTs, a malignant counterpart of these benign tumors, can also occur at the chest wall. The imaging features of these tumors are identical to those of similar tumors in other locations.

Schwannoma.—Schwannomas typically occur in patients between 20 and 50 years of age. They are almost invariably slow-growing nonaggressive neoplasms and usually manifest clinically as a painless mass (often <5 cm) without neurologic symptoms (43). Antoni A and Antoni B regions (Antoni A is a more organized hypercellular region composed of spindle cells, whereas Antoni B is a less organized hypocellular region demonstrating myxoid components) are the histologic hallmarks of schwannoma. Large schwannomas commonly undergo degenerative changes and demonstrate cyst formation, hemorrhage, calcification, and fibrosis. These features are far less common in neurofibroma (43).

Neurofibroma.—Neurofibromas most commonly develop in patients between 20 and 30 years of age and may demonstrate a localized, diffuse, or plexiform pattern. The localized type is by far the most common, representing approximately 90% of lesions, with the vast majority being solitary and not associated with neurofibromatosis type I. The diffuse type is associated with a plaquelike elevation of the skin and thickening of the entire

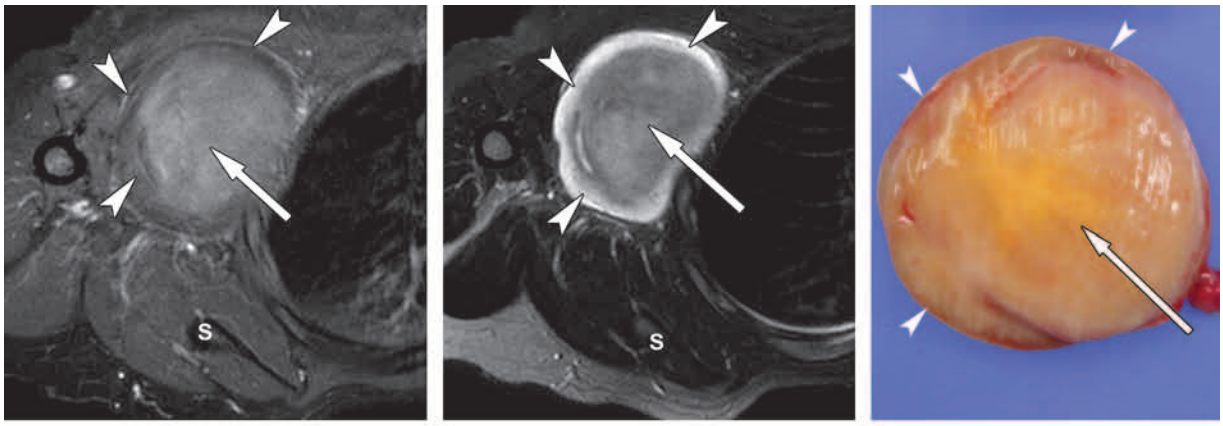

Figure 12. Neurofibroma in a 37-year-old woman. **(a)** Axial gadolinium-enhanced fat-suppressed T1-weighted MR image (600/9) obtained at the level of the end of the scapula *(S)* shows a lesion with central enhancement (arrow) and peripheral hypoenhancement (arrowheads). **(b)** Axial fat-suppressed T2-weighted MR image (5000/120) obtained at the same level shows a well-circumscribed mass. The central portion of the mass (arrow) has heterogeneous low signal intensity, whereas the tumor periphery (arrowheads) has high signal intensity, creating the so-called target sign. *S* = scapula. **(c)** Photograph of the cut surface of the excised specimen shows a well-circumscribed, yellowish myxoid mass (arrowheads) with central fibrovascular tissue (arrow), findings that correspond to the target sign seen at MR imaging.

subcutis. Plexiform neurofibromas diffusely involve long segments of a nerve and its branches and have a "bag of worms" appearance. The histologic appearance of solitary localized neurofibroma differs markedly from that of schwannoma. Neurofibromas do not contain Antoni A or Antoni B regions, and degenerative regions are not as prominent as in schwannomas (43). Furthermore, unlike schwannomas, neurofibromas are intimately intermixed and inseparable from affected nerve tissues, so that complete excision requires sacrifice of the affected nerve (44). Consequently, differentiation between these two entities is crucial, particularly when lesions are deep seated and involve nerves whose resection would cause severe functional compromise.

Imaging Features of Schwannoma vs Neurofibroma.—MR imaging has been proposed for the differential diagnosis of PNSTs. The classic target sign seen at T2-weighted imaging consists of relatively low signal intensity at the center of a lesion together with high signal intensity at the periphery. Typically, the central lower-signal-intensity region enhances on gadolinium-enhanced MR images, whereas the peripheral high-signal-intensity region does not (Fig 12). These MR imaging features correspond to pathologic findings of fibrovascular tissue (with high collagen content) centrally and more myxoid tissue peripherally (45). The target sign has been reported to be present at T2-weighted imaging in 50%–70% of neurofibromas and 0%–54% of schwannomas (45–47). Furthermore, the target sign on T2-weighted images and central enhancement on gadolinium-enhanced T1-weighted images have been reported to favor a diagnosis of neurofibroma (63% of cases) rather than schwannoma (3%) (46). In addition, the fascicular sign is seen at T2-weighted imaging and consists of heterogeneous low signal intensity with a ringlike pattern (Fig 13). One study reported that the fascicular sign was present in 63% of schwannomas and 25% of neurofibromas (47). However, there is considerable overlap between the imaging features of these two disease entities.

Malignant PNST.—Malignant PNSTs account for 5%–10% of all soft-tissue sarcomas and affect adults between 20 and 50 years of age. They are associated with neurofibromatosis type I in 25%–70% of cases and show a distinct propensity for affecting major or medium-sized nerves, including the sciatic nerve and the brachial and sacral plexuses. Differentiation between a malignant PNST and a benign neurogenic tumor is not difficult when the tumor is sufficiently large and infiltrative (Fig 14). However, it is not easy to differentiate a large, infiltrative malignant PNST from other sarcomas, unless the mass demonstrates certain imaging features, such as a location along the course of a large nerve or an intermuscular distribution ("split fat sign") (48).

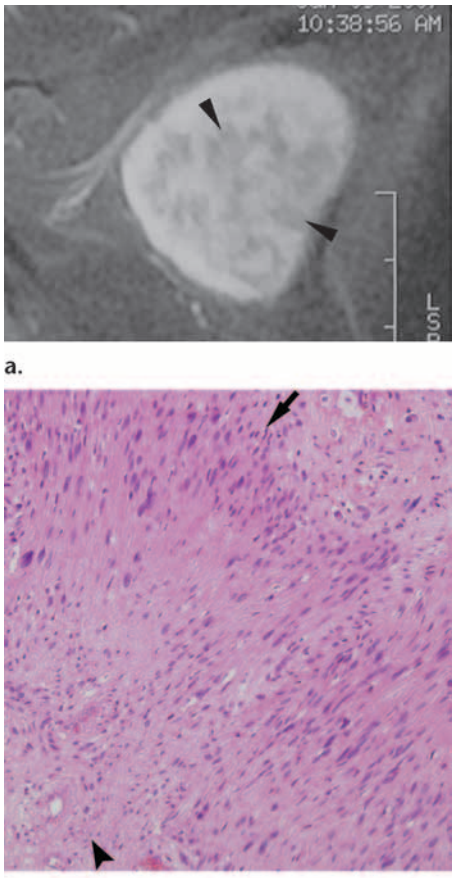

Figure 13. Schwannoma in a 66-year-old man. **(a)** Axial fat-suppressed T2-weighted MR image (3500/80) shows a well-circumscribed mass lateral to the rib cage. Diffusely scattered areas of heterogeneous signal intensity with a ringlike pattern (arrowheads) are seen against a hyperintense tumor background (fascicular sign). **(b)** Photomicrograph (original magnification, ×100; H-E stain) exhibits an Antoni A zone of hypercellularity composed of spindle cells (arrow) and an Antoni B zone of hypocellularity demonstrating myxoid components (arrowhead).

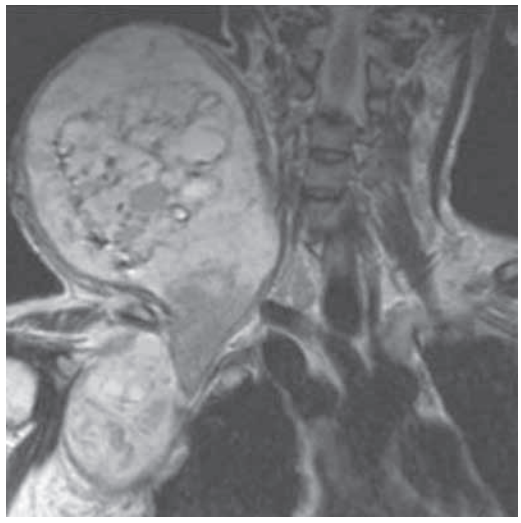

Figure 14. Malignant PNST in a 43-year-old woman who was referred for management of a large mass (maximum diameter, ~13 cm) at the neck wall that had grown through the upper chest wall. Coronal T2-weighted MR image (4000/80) obtained at the level of the thoracic inlet reveals a dumbbell-shaped mass with heterogeneous signal intensity.

Furthermore, the differentiation of malignant PNSTs from benign neurogenic tumors is sometimes difficult. MR imaging findings that favor a diagnosis of malignant PNST include a size over 5 cm, the absence of the target sign or fascicular sign, the presence of an ill-defined margin, and rapid interval growth on follow-up images (43).

Cutaneous Lesions

When imaging seems to indicate that a lesion originated from cutaneous tissue, the differential diagnosis includes epidermal inclusion cyst, pilomatricoma, and dermatofibrosarcoma protuberans (DFSP), along with cutaneous hemangioma and granuloma annulare, which are not discussed in this article.

Epidermal Inclusion Cyst.—Epidermal inclusion cysts result from a proliferation of epidermal cells within a circumscribed dermal space. The dermal space fills with keratin debris and is bounded by a wall of stratified squamous epithelium, resulting in the formation of a cyst. Epidermal inclusion cysts involve the scalp, face, neck, trunk, and back in more than 90% of cases (49) and are frequently observed on the chest wall. These cysts demonstrate characteristic MR imaging findings, including *(a)* a well-demarcated mass with variable low signal intensity with or without a cystlike high-signal-intensity background on T2-weighted images, *(b)* hyperintense foci on T1-weighted images, and *(c)* peripheral thin rim enhancement. It has been suggested that the hyperintense foci observed on T1-weighted images represent calcium components. The variable low signal intensity observed on T2-weighted images has been reported to be due to various components contained within the cyst (Fig 15). These characteristics, which are not typical of other masses with high water content, help differentiate epidermal inclusion cysts from other cystic lesions (50).

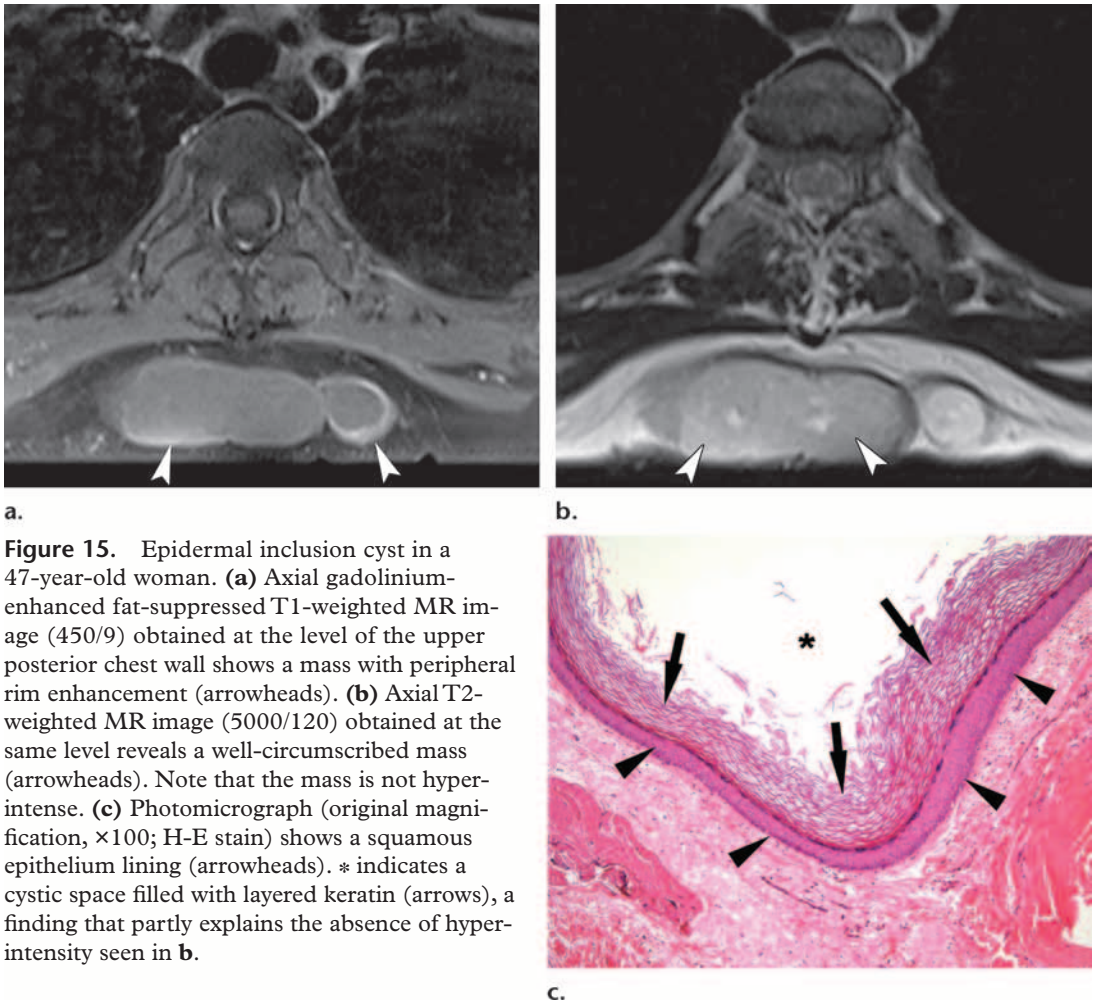

Figure 15. Epidermal inclusion cyst in a 47-year-old woman. **(a)** Axial gadolinium-enhanced fat-suppressed T1-weighted MR image (450/9) obtained at the level of the upper posterior chest wall shows a mass with peripheral rim enhancement (arrowheads). **(b)** Axial T2-weighted MR image (5000/120) obtained at the same level reveals a well-circumscribed mass (arrowheads). Note that the mass is not hyperintense. **(c)** Photomicrograph (original magnification, ×100; H-E stain) shows a squamous epithelium lining (arrowheads). * indicates a cystic space filled with layered keratin (arrows), a finding that partly explains the absence of hyperintensity seen in **b**.

Pilomatricoma.—Pilomatricomas, formerly known as pilomatrixomas, are benign subcutaneous tumors that arise from hair matrix and are most commonly found in children and young adults (51). They are typically located on the head and neck (68% of cases), with 29% seen on the trunk and 17% on the extremities (52). Pilomatricomas have a superficial location and typically manifest as subcutaneous or dermal nodules. At pathologic analysis, they are seen to consist of epithelial cells with basophilic cytoplasm arranged in an arclike fashion at the periphery (basaloid cells). In time, these cells are transformed into shadow cells (also known as ghost cells), which are more centrally located. These eosinophilic cells have no nuclei and are filled with keratin. The intracellular stroma is collagenous and contains dilated blood vessels (53). Pilomatricomas typically have homogeneous intermediate signal intensity on T1-weighted MR images and heterogeneous intermediate signal intensity on T2-weighted images, and they are considered to be covered with a connective tissue capsule, which enhances after gadolinium administration. However, the center of the lesion does not enhance prominently, with the exception of septa. Peritumoral edema or inflammation can also be identified at MR imaging (Fig 16). Calcium deposition commonly occurs in the shadow cell region and stroma (69%–85% of cases) (53). When calcification occurs, the radiologic differential diagnosis includes a calcified lymph node, ossifying hematoma, and hemangioma with phlebolith. Granuloma annulare and DFSP, both of which have a superficial location, are also included in the differential diagnosis, but both manifest as soft-tissue masses without calcification (54).

Teaching Point

Dermatofibrosarcoma Protuberans.—DFSP is an uncommon spindle cell tumor that arises in the dermis and typically spreads into subcutaneous tissues and muscles. It is no longer classified as a soft-tissue tumor by the WHO, but rather as

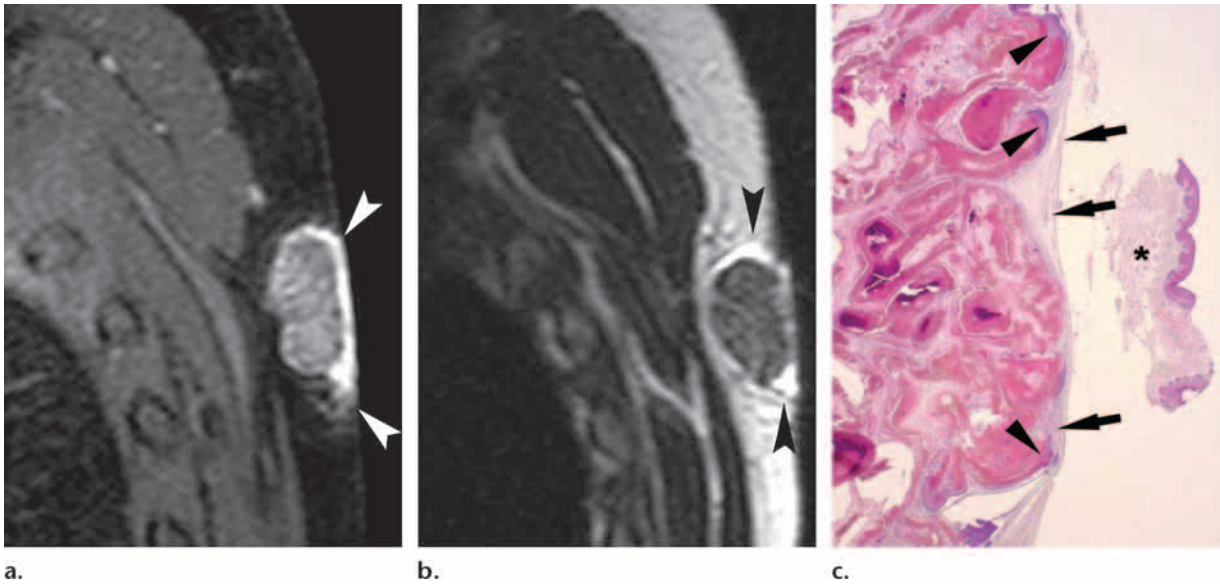

Figure 16. Pilomatricoma in a 9-year-old boy. **(a)** Sagittal gadolinium-enhanced fat-suppressed T1-weighted MR image (550/9) obtained at the level of the upper posterior chest wall shows a nodule with diffuse reticular enhancement. Note the intense enhancement of the fibrous capsule at the periphery on the dermal side of the lesion (arrowheads). **(b)** Sagittal T2-weighted MR image (3000/90) obtained adjacent to **a** shows a well-circumscribed subcutaneous nodule that is hyperintense relative to adjacent muscle. The increased signal intensity surrounding the nodule (arrowheads) suggests peritumoral edema. **(c)** Photomicrograph (original magnification, ×12; H-E stain) reveals nucleated basaloid cells (arrowheads) under a capsule of compressed fibrous tissue (arrows) deep to the dermis (*). The fibrous capsule corresponds to the area of enhancement seen at the lesion periphery in **a**.

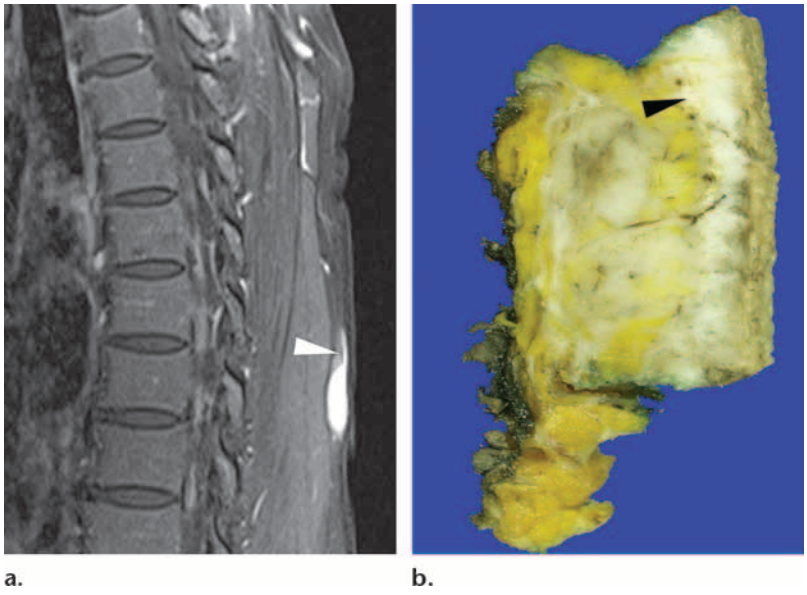

Figure 17. DFSP in a 46-year-old woman. **(a)** Sagittal gadolinium-enhanced fat-suppressed T1-weighted MR image (550/9) shows an intensely enhancing nodule at the posterior chest wall that extends along and invades the deep layer of the dermis (arrowhead). **(b)** Photograph of the cut surface of the excised specimen shows ill-defined whitish tumor tissue (arrowhead) extending along the deep layer of the dermis, a finding that corresponds to the linear enhancing lesion seen in **a**.

a skin tumor (3). Because of the layer in which this entity occurs, we consider it to be a soft-tissue tumor originating from a cutaneous layer. The trunk is the most common site of involvement (almost 50% of cases) (55). DFSP typically occurs in adolescents, although it may occur much later in life. At CT, this tumor manifests as a well-defined nodular subcutaneous lesion without calcification. MR imaging findings of DFSP vary from a small nodule to a large mass abutting the dermis. The intrinsic MR imaging findings are nonspecific and include hypointensity on T1-weighted images (Fig 17) and hyperintensity relative to fat on T2-weighted images (56). DFSP lesions may include heterogeneous foci of hemorrhage, myxoid change, or necrosis (55).

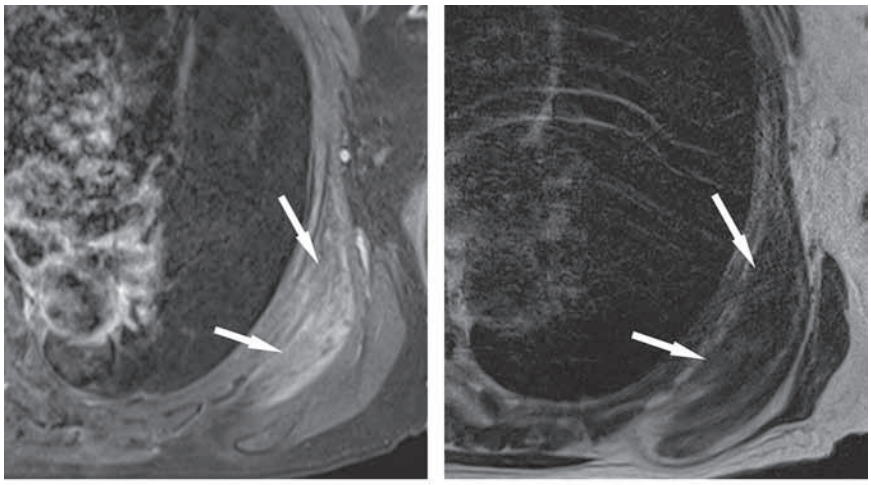

Figure 18. Elastofibroma in a 78-year-old woman. **(a)** Axial gadolinium-enhanced fat-suppressed T1-weighted MR image (550/9) shows a crescent-shaped soft-tissue lesion with diffuse streaky enhancement (arrows) in the deep dorsal region between the thoracic wall and the lower third of the scapula. **(b)** On an axial T2-weighted MR image (4500/120), the mass (arrows) is mostly isointense relative to adjacent muscle, with interspersed streaks of hyperintense fat.

Fibroblastic-Myofibroblastic Tumors

Of the numerous fibroblastic-myofibroblastic tumors, we discuss two in this article: elastofibroma dorsi and fibromatosis.

Elastofibroma Dorsi.—Elastofibroma dorsi is a pseudotumor of the soft tissue with a 4:1 female predilection. The average patient age at onset is 60 years (range, 41–80 years). In one investigation, most lesions (93%) were reported to occur in deep dorsal regions between the thoracic wall and the lower third of the scapula under the serratus anterior and latissimus dorsi muscles (57). These lesions are often asymptomatic, and bilaterality is common (10%–66% of cases) (58). At MR imaging, elastofibroma dorsi typically manifests as a mass with a signal intensity similar to that of muscle on both T1- and T2-weighted images, with interspersed streaks of fat in a fascicular pattern (Fig 18) (59).

Fibromatosis.—Fibromatosis, or desmoid tumor, is considered to be a true neoplasm and is composed of well-differentiated fibroblasts embedded in an abundant collagenous matrix with increased cellularity at the periphery (60). It arises from connective tissue in muscle, fascia, or aponeurosis, or sometimes at the site of a traumatic or postsurgical scar. Generally, fibromatosis is poorly circumscribed, nonencapsulated, and infiltrative, and grows insidiously. Although the lesion is locally aggressive, it is not malignant and does not metastasize. The chest wall has been reported to be the site of origin in 10%–28% of cases (9). Fibromatosis often affects adolescents and young adults (Fig 19) but may also occur in older patients. At CT, fibromatosis may be poorly defined, suggesting aggressiveness, and may show variable attenuation and enhancement owing to varying degrees of cellularity, matrix water content, and infiltration (61). At MR imaging, fibromatosis usually has heterogeneous signal intensity, which probably reflects different amounts and distributions of spindle-shaped cells, extracellular collagen, and myxoid matrix. In one report, T2-weighted imaging depicted hypointense bands in 86% of cases of fibromatosis, a finding that probably corresponded to dense conglomerations of collagen bundles, which were observed histologically (62). These collagen bundles do not enhance after contrast material administration, although tumors typically show moderate to marked heterogeneous enhancement (63).

So-called Fibrohistiocytic Tumors

UPS is classified as a fibrohistiocytic tumor by the WHO (3). It is a pleomorphic soft-tissue sarcoma that arises in deep fascia or skeletal muscle and is the most common malignant soft-tissue tumor in adults (58), although its imaging features are nonspecific. It tends to be found on the thigh, on the trunk, or in the retroperitoneum, but is found only rarely at the chest wall. Clinical cases show a slight female predilection and a mean patient age of 55 years at onset (64). According to the WHO classification system, there are three histologic subtypes of UPS: high-grade pleomorphic sarcoma, pleomorphic sarcoma with giant cells, and pleomorphic sarcoma with prominent inflammation.

Before describing the imaging features of UPS, we should address myxoid malignant fibrous histiocytoma, which was previously considered to

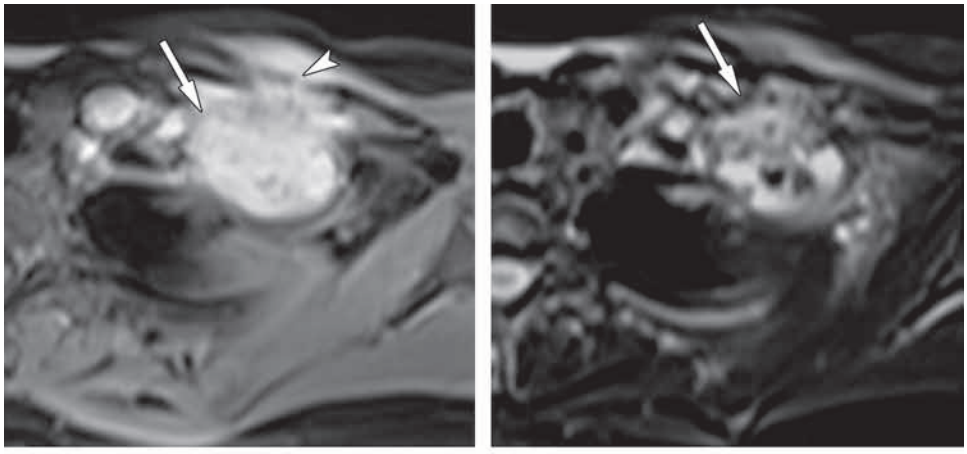

a. b.

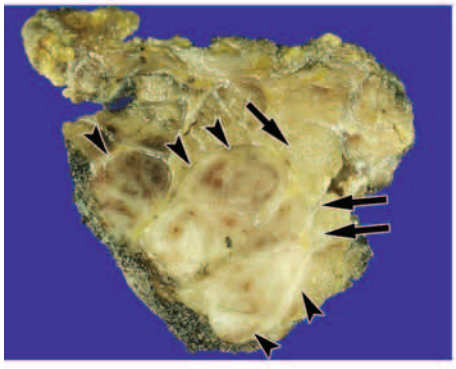

c.

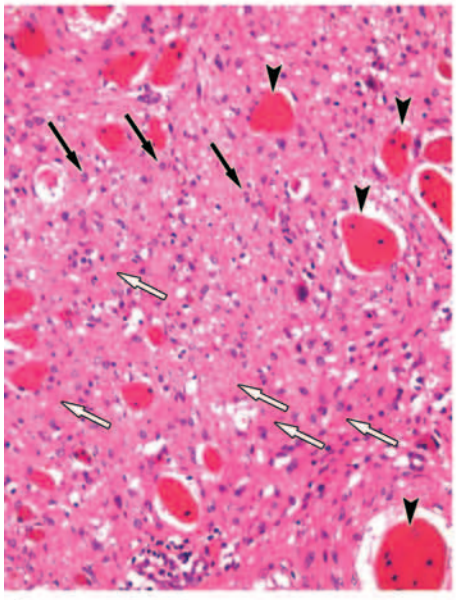

d.

Figure 19. Fibromatosis in a 19-year-old woman. **(a)** Axial gadolinium-enhanced fat-suppressed T1-weighted MR image (650/9) obtained at the level of the clavicle shows a mass with diffuse intense but heterogeneous enhancement (arrow) and obvious infiltration into the adjacent pectoralis major muscle (arrowhead). **(b)** Axial fat-suppressed T2-weighted MR image (3500/95) obtained at the same level shows the mass (arrow) with intermediate signal intensity. The signal voids within the mass are suggestive of fibrous collagen bands. **(c)** Photograph of the cut surface of the excised specimen shows the mass with a lobular contour (arrowheads) and a white-gray rubbery texture. Note the infiltration of whitish fibrous tissues into adjacent muscle (arrows). **(d)** Photomicrograph (original magnification, ×200; H-E stain) shows fibroblasts (black arrows) scattered throughout a background of collagenous fibers (white arrows). Note the smooth muscle cells (arrowheads), which suggest tumor infiltration of the adjacent muscle.

be a subtype of UPS. Myxoid malignant fibrous histiocytoma is now referred to as myxofibrosarcoma and is categorized as a fibroblastic-myofibroblastic tumor rather than a fibrohistiocytic tumor (37). However, we describe the imaging findings of UPS and myxofibrosarcoma together because these findings overlap, although they sometimes reflect histologic differences.

At CT, UPS manifests as nonspecific, heterogeneously enhancing masses in muscle and fascial planes, whereas myxofibrosarcoma typically demonstrates a hypoattenuating central region with peripheral nodular enhancement, reflecting a central myxoid matrix and greater peripheral cellularity (9). Although calcification or ossification has been reported at the lesion periphery in a small percentage of cases of UPS, calcification is generally considered unusual except in previously treated cases (9,27,64). At MR imaging, the signal intensity of soft-tissue fibrous malignancies

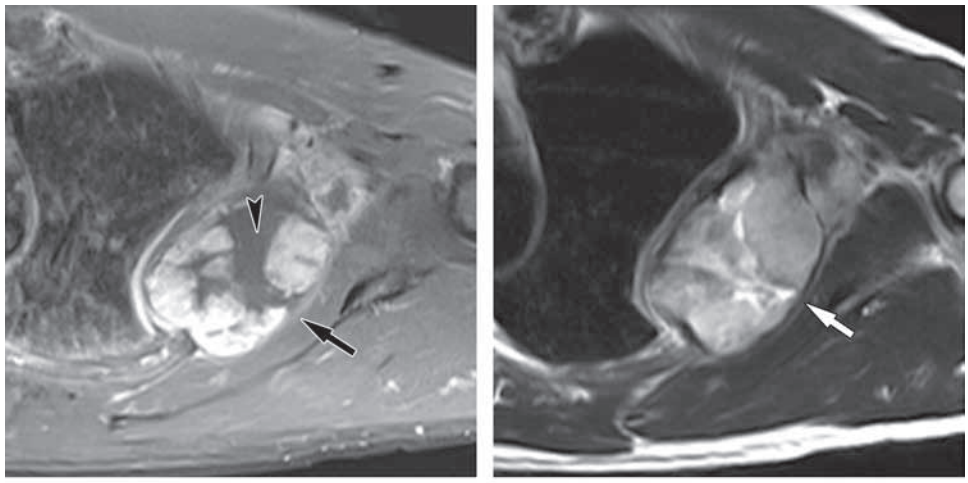

a. b.

Figure 20. UPS in a 58-year-old man. **(a)** Axial gadolinium-enhanced fat-suppressed T1-weighted MR image (550/9) obtained at the level of the aortic arch shows a strongly enhancing mass (arrow) with a central nonenhanced region (arrowhead) that is suggestive of necrosis. **(b)** Axial T2-weighted MR image (4500/120) obtained at the same level shows the mass (arrow) with nonspecific heterogeneous signal intensity that is higher than that of adjacent muscle and lower than that of subcutaneous fat tissue.

is typically intermediate to low on T1-weighted images and intermediate to high on T2-weighted images (Fig 20). Variations in signal intensity are believed to correlate with various fibrous tissue components with high collagen content (low signal intensity with all pulse sequences), myxoid tissue (low signal intensity on T1-weighted images and high signal intensity on T2-weighted images), and hemorrhage (variable signal intensity) (37).

Summary

The presence of a bone lesion in the chest wall with locally aggressive features and mineralization suggests the diagnosis of chondrosarcoma, whereas nonmineralization should raise suspicion for metastasis or myeloma. A benign-appearing bone lesion involving the chest wall should initially be considered to represent fibrous dysplasia or osteochondroma. In primary soft-tissue masses of the chest wall, MR imaging findings of thick septa, nodular enhancement on contrast-enhanced T1-weighted images, and a nonadipose component involving more than 25% of the mass favor a diagnosis of liposarcoma rather than lipoma. The target sign and fascicular sign are useful MR imaging findings of PNST but are not pathognomonic for neurofibroma or schwannoma, respectively, and do not allow the differentiation of benign from malignant PNSTs. Serpentine vascular channels, phleboliths, and fat foci are diagnostic for hemangioma. A superficial aggressive tumor associated with lymphedema suggests angiosarcoma. Subcutaneous lesions that originate from the skin suggest epidermal inclusion cyst, pilomatricoma, or DFSP as a likely diagnosis. On the other hand, elastofibroma occurs at the lower tip of the scapula and is likely to be bilateral.

References

1. O'Sullivan P, O'Dwyer H, Flint J, Munk PL, Muller NL. Malignant chest wall neoplasms of bone and cartilage: a pictorial review of CT and MR findings. Br J Radiol 2007;80(956):678–684.
2. O'Sullivan P, O'Dwyer H, Flint J, Munk PL, Muller N. Soft tissue tumours and mass-like lesions of the chest wall: a pictorial review of CT and MR findings. Br J Radiol 2007;80(955):574–580.
3. Fletcher CDM, Unni KK, Mertens F. Pathology and genetics of tumours of soft tissue and bone. In: World Health Organization classification of tumours. Lyon, France: IARC, 2002; 9–224.
4. Greenspan A, Jundt G, Remagen W. Metastases. In: Greenspan A, Jundt G, Remagen W, eds. Differential diagnosis in orthopaedic oncology. 2nd ed. Philadelphia, Pa: Lippincott Williams & Wilkins, 2007; 458–480.
5. Teitelbaum SL. Twenty years' experience with intrinsic tumors of the bony thorax at a large institution. J Thorac Cardiovasc Surg 1972;63(5):776–782.
6. Waller DA, Newman RJ. Primary bone tumours of the thoracic skeleton: an audit of the Leeds regional bone tumour registry. Thorax 1990;45(11): 850–855.

7. Lee TJ, Collins J. MR imaging evaluation of disorders of the chest wall. Magn Reson Imaging Clin N Am 2008;16(2):355–379, x.
8. Kuhlman JE, Bouchardy L, Fishman EK, Zerhouni EA. CT and MR imaging evaluation of chest wall disorders. RadioGraphics 1994;14(3):571–595.
9. Tateishi U, Gladish GW, Kusumoto M, et al. Chest wall tumors: radiologic findings and pathologic correlation. II. Malignant tumors. RadioGraphics 2003; 23(6):1491–1508.
10. Meyer CA, White CS. Cartilaginous disorders of the chest. RadioGraphics 1998;18(5):1109–1123.
11. Anderson BO, Burt ME. Chest wall neoplasms and their management. Ann Thorac Surg 1994;58(6): 1774–1781.
12. Ehara S, Nakayama T, Nishida J, Shiraishi H, Yoshioka H, Aoki J. Bone scintigraphic and CT evaluation of chondrosarcoma of the rib: correlation with histological grade in 6 cases. Ann Nucl Med 2004; 18(7):633–636.
13. McFarland GB Jr, McKinley LM, Reed RJ. Dedifferentiation of low grade chondrosarcomas. Clin Orthop Relat Res 1977 (122):157–164.
14. Park YK, Ryu KN. Parosteal osteosarcoma of the scapula. J Korean Med Sci 1999;14(5):586–588.
15. Unni KK. Osteosarcoma. In: Unni KK, ed. Dahlin's bone tumors: general aspects and data on 11,087 cases. 5th ed. Philadelphia, Pa: Lippincott-Raven, 1996; 147.
16. Berquist TH. Magnetic resonance imaging of primary skeletal neoplasms. Radiol Clin North Am 1993;31(2):411–424.
17. Bohndorf K, Reiser M, Lochner B, Féaux de Lacroix W, Steinbrich W. Magnetic resonance imaging of primary tumours and tumour-like lesions of bone. Skeletal Radiol 1986;15(7):511–517.
18. Incarbone M, Pastorino U. Surgical treatment of chest wall tumors. World J Surg 2001;25(2): 218–230.
19. Hughes EK, James SL, Butt S, Davies AM, Saifuddin A. Benign primary tumours of the ribs. Clin Radiol 2006;61(4):314–322.
20. Jee WH, Choi KH, Choe BY, Park JM, Shinn KS. Fibrous dysplasia: MR imaging characteristics with radiopathologic correlation. AJR Am J Roentgenol 1996;167(6):1523–1527.
21. Ogawa K, Yoshida A, Ui M. Symptomatic osteochondroma of the clavicle: a report of two cases. J Bone Joint Surg Am 1999;81(3):404–408.
22. Tang WM, Luk KD, Leong JC. Costal osteochondroma: a rare cause of spinal cord compression. Spine (Phila Pa 1976) 1998;23(17):1900–1903.
23. Tateishi U, Gladish GW, Kusumoto M, et al. Chest wall tumors: radiologic findings and pathologic correlation. I. Benign tumors. RadioGraphics 2003;23 (6):1477–1490.
24. Okada K, Terada K, Sashi R, Hoshi N. Large bursa formation associated with osteochondroma of the scapula: a case report and review of the literature. Jpn J Clin Oncol 1999;29(7):356–360.
25. Woertler K, Lindner N, Gosheger G, Brinkschmidt C, Heindel W. Osteochondroma: MR imaging of tumor-related complications. Eur Radiol 2000;10(5): 832–840.
26. Jeung MY, Gangi A, Gasser B, et al. Imaging of chest wall disorders. RadioGraphics 1999;19(3): 617–637.
27. Gladish GW, Sabloff BM, Munden RF, Truong MT, Erasmus JJ, Chasen MH. Primary thoracic sarcomas. RadioGraphics 2002;22(3):621–637.
28. Mayo-Smith W, Rosenberg AE, Khurana JS, Kattapuram SV, Romero LH. Chondroblastoma of the rib: a case report and review of the literature. Clin Orthop Relat Res 1990 (251):230–234.
29. Beltran J, Simon DC, Levy M, Herman L, Weis L, Mueller CF. Aneurysmal bone cysts: MR imaging at 1.5 T. Radiology 1986;158(3):689–690.
30. Hudson TM, Hamlin DJ, Fitzsimmons JR. Magnetic resonance imaging of fluid levels in an aneurysmal bone cyst and in anticoagulated human blood. Skeletal Radiol 1985;13(4):267–270.
31. Murphey MD, Nomikos GC, Flemming DJ, Gannon FH, Temple HT, Kransdorf MJ. Imaging of giant cell tumor and giant cell reparative granuloma of bone: radiologic-pathologic correlation. RadioGraphics 2001;21(5):1283–1309.
32. Kwon JW, Chung HW, Cho EY, et al. MRI findings of giant cell tumors of the spine. AJR Am J Roentgenol 2007;189(1):246–250.
33. Woertler K. Benign bone tumors and tumor-like lesions: value of cross-sectional imaging. Eur Radiol 2003;13(8):1820–1835.
34. Bancroft LW, Kransdorf MJ, Peterson JJ, O'Connor MI. Benign fatty tumors: classification, clinical course, imaging appearance, and treatment. Skeletal Radiol 2006;35(10):719–733.
35. Kransdorf MJ, Bancroft LW, Peterson JJ, Murphey MD, Foster WC, Temple HT. Imaging of fatty tumors: distinction of lipoma and well-differentiated liposarcoma. Radiology 2002;224(1):99–104.
36. Kransdorf MJ. Malignant soft-tissue tumors in a large referral population: distribution of diagnoses by age, sex, and location. AJR Am J Roentgenol 1995;164(1):129–134.
37. Murphey MD. World Health Organization classification of bone and soft tissue tumors: modifications and implications for radiologists. Semin Musculoskelet Radiol 2007;11(3):201–214.
38. Hosono M, Kobayashi H, Fujimoto R, et al. Septum-like structures in lipoma and liposarcoma: MR imaging and pathologic correlation. Skeletal Radiol 1997;26(3):150–154.
39. Peterson JJ, Kransdorf MJ, Bancroft LW, O'Connor MI. Malignant fatty tumors: classification, clinical course, imaging appearance and treatment. Skeletal Radiol 2003;32(9):493–503.
40. Kransdorf MJ, Murphey MD. Vascular and lymphatic tumors. In: Kransdorf MJ, Murphey MD, eds. Imaging of soft tissue tumors. 2nd ed. Philadelphia, Pa: Lippincott Williams & Wilkins, 2006; 150–188.
41. Mulliken JB, Glowacki J. Hemangiomas and vascular malformations in infants and children: a classification based on endothelial characteristics. Plast Reconstr Surg 1982;69(3):412–422.

42. Levine E, Wetzel LH, Neff JR. MR imaging and CT of extrahepatic cavernous hemangiomas. AJR Am J Roentgenol 1986;147(6):1299–1304.
43. Kransdorf MJ, Murphey MD. Neurogenic tumors. In: Kransdorf MJ, Murphey MD, eds. Imaging of soft tissue tumors. 2nd ed. Philadelphia, Pa: Lippincott Williams & Wilkins, 2006; 328–380.
44. Kehoe NJ, Reid RP, Semple JC. Solitary benign peripheral-nerve tumours: review of 32 years' experience. J Bone Joint Surg Br 1995;77(3):497–500.
45. Suh JS, Abenoza P, Galloway HR, Everson LI, Griffiths HJ. Peripheral (extracranial) nerve tumors: correlation of MR imaging and histologic findings. Radiology 1992;183(2):341–346.
46. Jee WH, Oh SN, McCauley T, et al. Extraaxial neurofibromas versus neurilemmomas: discrimination with MRI. AJR Am J Roentgenol 2004;183(3): 629–633.
47. Varma DG, Moulopoulos A, Sara AS, et al. MR imaging of extracranial nerve sheath tumors. J Comput Assist Tomogr 1992;16(3):448–453.
48. Van Herendael BH, Heyman SR, Vanhoenacker FM, et al. The value of magnetic resonance imaging in the differentiation between malignant peripheral nerve-sheath tumors and non-neurogenic malignant soft-tissue tumors. Skeletal Radiol 2006;35(10): 745–753.
49. Vincent LM, Parker LA, Mittelstaedt CA. Sonographic appearance of an epidermal inclusion cyst. J Ultrasound Med 1985;4(11):609–611.
50. Hong SH, Chung HW, Choi JY, Koh YH, Choi JA, Kang HS. MRI findings of subcutaneous epidermal cysts: emphasis on the presence of rupture. AJR Am J Roentgenol 2006;186(4):961–966.
51. Pirouzmanesh A, Reinisch JF, Gonzalez-Gomez I, Smith EM, Meara JG. Pilomatrixoma: a review of 346 cases. Plast Reconstr Surg 2003;112(7): 1784–1789.
52. Laffan EE, Ngan BY, Navarro OM. Pediatric soft-tissue tumors and pseudotumors: MR imaging features with pathologic correlation. II. Tumors of fibroblastic/myofibroblastic, so-called fibrohistiocytic, muscular, lymphomatous, neurogenic, hair matrix, and uncertain origin. RadioGraphics 2009;29(4):e36.
53. Lan MY, Lan MC, Ho CY, Li WY, Lin CZ. Pilomatricoma of the head and neck: a retrospective review of 179 cases. Arch Otolaryngol Head Neck Surg 2003;129(12):1327–1330.
54. Lim HW, Im SA, Lim GY, et al. Pilomatricomas in children: imaging characteristics with pathologic correlation. Pediatr Radiol 2007;37(6):549–555.
55. Kransdorf MJ, Meis-Kindblom JM. Dermatofibrosarcoma protuberans: radiologic appearance. AJR Am J Roentgenol 1994;163(2):391–394.
56. Torreggiani WC, Al-Ismail K, Munk PL, Nicolaou S, O'Connell JX, Knowling MA. Dermatofibrosarcoma protuberans: MR imaging features. AJR Am J Roentgenol 2002;178(4):989–993.
57. Nagamine N, Nohara Y, Ito E. Elastofibroma in Okinawa: a clinicopathologic study of 170 cases. Cancer 1982;50(9):1794–1805.
58. Kransdorf MJM, Murphey MD. Benign fibrous and fibrohistiocytic tumors. In: Kransdorf MJ, Murphey MD, eds. Imaging of soft tissue tumors. 2nd ed. Philadelphia, Pa: Lippincott Williams & Wilkins, 2006; 189–256.
59. Battaglia M, Vanel D, Pollastri P, et al. Imaging patterns in elastofibroma dorsi. Eur J Radiol 2009;72 (1):16–21.
60. Bridge JA, Sreekantaiah C, Mouron B, Neff JR, Sandberg AA, Wolman SR. Clonal chromosomal abnormalities in desmoid tumors: implications for histopathogenesis. Cancer 1992;69(2):430–436.
61. Ackman JB, Whitman GJ, Chew FS. Aggressive fibromatosis. AJR Am J Roentgenol 1994;163(3):544.
62. Kransdorf MJ, Jelinek JS, Moser RP Jr, et al. Magnetic resonance appearance of fibromatosis: a report of 14 cases and review of the literature. Skeletal Radiol 1990;19(7):495–499.
63. Dinauer PA, Brixey CJ, Moncur JT, Fanburg-Smith JC, Murphey MD. Pathologic and MR imaging features of benign fibrous soft-tissue tumors in adults. RadioGraphics 2007;27(1):173–187.
64. Tateishi U, Kusumoto M, Hasegawa T, Yokoyama R, Moriyama N. Primary malignant fibrous histiocytoma of the chest wall: CT and MR appearance. J Comput Assist Tomogr 2002;26(4):558–563.

Imaging of Primary Chest Wall Tumors with Radiologic-Pathologic Correlation[1]

Se Jin Nam, MD • Sungjun Kim, MD • Beom Jin Lim, MD • Choon-Sik Yoon, MD • Tae Hoon Kim, MD • Jin-Suck Suh, MD • Doo Hoe Ha, MD Jong Won Kwon, MD • Young Cheol Yoon, MD • Hye Won Chung, MD • Mi Sook Sung, MD • Yun Sun Choi, MD • Jang Gyu Cha, MD

RadioGraphics 2011; 31:749–770 • **Published online** 10.1148/rg.313105509 • **Content Codes:** CH MK

Page 752
Chondrosarcoma is the most common primary malignant bone tumor of the chest wall and accounts for 33% of all primary rib tumors, with myeloma being the second most common. Ewing sarcoma is the most common primary bone tumor in children (1,8–10). Fibrous dysplasia is the most common benign tumorous condition of the osseous chest wall, accounting for approximately 30% of these tumors (11).

Page 757
However, enchondroma is generally considered to occur only rarely on the chest wall (7,26); chondrosarcoma is much more common. Hence, a destructive osseous lesion of the chest wall is initially suspected by the radiologist to be chondrosarcoma when mineralization is present (27).

Page 758
In adults, the most common benign soft-tissue neoplasm is lipoma, and the most common malignant neoplasm is undifferentiated pleomorphic sarcoma (UPS), a term that is used interchangeably with *malignant fibrous histiocytoma*. In children, rhabdomyosarcoma and primitive neuroectodermal tumor (Askin tumor) are the most common malignant soft-tissue tumors (26).

Page 759 (Figure on page 759)
MR imaging features that suggest well-differentiated liposarcoma rather than lipoma include the presence of *(a)* prominent internal septa greater than 2 mm in thickness, and *(b)* nodular nonadipose areas (35). The gadolinium enhancement of nonadipose regions is variable (Fig 9) and has been described as ranging from mild to marked (35); however, one research group reported that the thick, irregular septa of liposarcomas enhance significantly in most cases, whereas thin septa enhance only faintly (38).

Page 764
Calcium deposition commonly occurs in the shadow cell region and stroma (69%–85% of cases) (53). When calcification occurs, the radiologic differential diagnosis includes a calcified lymph node, ossifying hematoma, and hemangioma with phlebolith. Granuloma annulare and DFSP, both of which have a superficial location, are also included in the differential diagnosis, but both manifest as soft-tissue masses without calcification (54).